EUROPEAN ORGANISATION FOR NUCLEAR RESEARCH

CERN-EP/90-100
9 July 1990

Searches for Neutral Higgs Bosons in e^+e^- Collisions at LEP

The OPAL Collaboration

Abstract

A search for Minimal Standard Model (MSM) and Minimal Supersymmetric Model (MSSM) Higgs bosons with masses larger than 3 GeV/c^2 has been performed by the OPAL collaboration on e^+e^- data from LEP corresponding to an integrated luminosity of 1.24 pb^{-1}. The limits for MSM Higgs bosons have been obtained using the channels $Z^0 \to Z^{0*}H^0$, $Z^{0*} \to (\nu\bar{\nu}$ *or* e^+e^- *or* $\mu^+\mu^-)$, $H^0 \to q\bar{q}$. The search for MSSM Higgs bosons has been performed using the channels $Z^0 \to Z^{0*}h^0$, $Z^{0*} \to (\nu\bar{\nu}$ *or* e^+e^- *or* $\mu^+\mu^-)$, $h^0 \to q\bar{q}$ and $Z^0 \to h^0A^0$, $h^0A^0 \to (4$ *jet or* $\tau^+\tau^-jj$ *or* $4\ \tau)$, where h^0 and A^0 are the two lightest neutral MSSM Higgs bosons.

No Higgs boson signal has been observed. The MSM Higgs boson is excluded in the mass range $3\ GeV < m_{H^0} < 25.3\ GeV/c^2$ at the 95% confidence level; limits on the masses of the two lightest neutral MSSM Higgs bosons are obtained for h^0 masses up to 40.5 GeV/c^2.

(Submitted to Zeit. Phys. C)

The OPAL Collaboration

M.Z. Akrawy[11], G. Alexander[21], J. Allison[14], P.P. Allport[5], K.J. Anderson[8], J.C. Armitage[6], G.T.J. Arnison[18], P. Ashton[14], G. Azuelos[16,f], J.T.M. Baines[14], A.H. Ball[15], J. Banks[14], G.J. Barker[11], R.J. Barlow[14], J.R. Batley[5], J. Becker[9], T. Behnke[7], K.W. Bell[18], G. Bella[21], S. Bethke[10], O. Biebel[3], U. Binder[9], I.J. Bloodworth[1], P. Bock[10], H. Breuker[7], R.M. Brown[18], R. Brun[7], A. Buijs[7], H.J. Burckhart[7], P. Capiluppi[2], R.K. Carnegie[6], A.A. Carter[11], J.R. Carter[5], C.Y. Chang[15], D.G. Charlton[7], J.T.M. Chrin[14], P.E.L. Clarke[23], I. Cohen[21], W.J. Collins[5], J.E. Conboy[13], M. Couch[1], M. Coupland[12], M. Cuffiani[2], S. Dado[20], G.M. Dallavalle[2], P. Debu[19], M.M. Deninno[2], A. Dieckmann[10], M. Dittmar[4], M.S. Dixit[17], E. Duchovni[24], I.P. Duerdoth[7,d], D. Dumas[6], H. El Mamouni[16], P.A. Elcombe[5], P.G. Estabrooks[6], E. Etzion[21], F. Fabbri[2], P. Farthouat[19], H.M. Fischer[3], D.G. Fong[15], M.T. French[18], C. Fukunaga[22], A. Gaidot[19], O. Ganel[24], J.W. Gary[10], J. Gascon[16], N.I. Geddes[18], C.N.P. Gee[18], C. Geich-Gimbel[3], S.W. Gensler[8], F.X. Gentit[19], G. Giacomelli[2], V. Gibson[5], W.R. Gibson[11], J.D. Gillies[18], J. Goldberg[20], M.J. Goodrick[5], W. Gorn[4], D. Granite[20], E. Gross[24], J. Grunhaus[21], H. Hagedorn[9], J. Hagemann[7], M. Hansroul[7], C.K. Hargrove[17], I. Harrus[20], J. Hart[5], P.M. Hattersley[1], M. Hauschild[7], C.M. Hawkes[7], E. Heflin[4], R.J. Hemingway[6], R.D. Heuer[7], J.C. Hill[5], S.J. Hillier[1], C. Ho[4], J.D. Hobbs[8], P.R. Hobson[23], D. Hochman[24], B. Holl[7], R.J. Homer[1], S.R. Hou[15], C.P. Howarth[13], R.E. Hughes-Jones[14], R. Humbert[9], P. Igo-Kemenes[10], H. Ihssen[10], D.C. Imrie[23], A. Jawahery[15], P.W. Jeffreys[18], H. Jeremie[16], M. Jimack[7], M. Jobes[1], R.W.L. Jones[11], P. Jovanovic[1], D. Karlen[6], K. Kawagoe[22], T. Kawamoto[22], R.G. Kellogg[15], B.W. Kennedy[13], C. Kleinwort[7], D.E. Klem[17], G. Knop[3], T. Kobayashi[22], T.P. Kokott[3], L. Köpke[7], R. Kowalewski[6], H. Kreutzmann[3], J. Kroll[8], M. Kuwano[22], P. Kyberd[11], G.D. Lafferty[14], F. Lamarche[16], W.J. Larson[4], J.G. Layter[4], P. Le Du[19], P. Leblanc[16], A.M. Lee[15], M.H. Lehto[13], D. Lellouch[7], P. Lennert[10], L. Lessard[16], L. Levinson[24], S.L. Lloyd[11], F.K. Loebinger[14], J.M. Lorah[15], B. Lorazo[16], M.J. Losty[17], J. Ludwig[9], J. Ma[4,b], A.A. Macbeth[14], M. Mannelli[7], S. Marcellini[2], G. Maringer[3], A.J. Martin[11], J.P. Martin[16], T. Mashimo[22], P. Mättig[7], U. Maur[3], T.J. McMahon[1], J.R. McNutt[13], A.C. McPherson[6,c], F. Meijers[7], D. Menszner[10], F.S. Merritt[8], H. Mes[17], A. Michelini[7], R.P. Middleton[18], G. Mikenberg[24], D.J. Miller[13], C. Milstene[21], M. Minowa[22], W. Mohr[9], A. Montanari[2], T. Mori[22], M.W. Moss[14], P.G. Murphy[14], W.J. Murray[5], B. Nellen[3], H.H. Nguyen[8], M. Nozaki[22], A.J.P. O'Dowd[14], S.W. O'Neale[7,e], B.P. O'Neill[4], F.G. Oakham[17], F. Odorici[2], M. Ogg[6], H. Oh[4], M.J. Oreglia[8], S. Orito[22], J.P. Pansart[19], G.N. Patrick[18], S.J. Pawley[14], P. Pfister[9], J.E. Pilcher[8], J.L. Pinfold[24], D.E. Plane[7], B. Poli[2], A. Pouladdej[6], T.W. Pritchard[11], G. Quast[7], J. Raab[7], M.W. Redmond[8], D.L. Rees[1], M. Regimbald[16], K. Riles[4], C.M. Roach[5], S.A. Robins[11], A. Rollnik[3], J.M. Roney[8], S. Rossberg[9], A.M. Rossi[2,a], P. Routenburg[6], K. Runge[9], O. Runolfsson[7], S. Sanghera[6], R.A. Sansum[18], M. Sasaki[22], B.J. Saunders[18], A.D. Schaile[9], O. Schaile[9], W. Schappert[6], P. Scharff-Hansen[7], S. Schreiber[3], J. Schwarz[9], A. Shapira[24], B.C. Shen[4], P. Sherwood[13], A. Simon[3], P. Singh[11], G.P. Siroli[2], A. Skuja[15], A.M. Smith[7], T.J. Smith[1], G.A. Snow[15], R.W. Springer[15], M. Sproston[18], K. Stephens[14], H.E. Stier[9], R. Stroehmer[10], D. Strom[8], H. Takeda[22], T. Takeshita[22], T. Tsukamoto[22], M.F. Turner[5], G. Tysarczyk-Niemeyer[10], D. Van den plas[16], G.J. VanDalen[4], G. Vasseur[19], C.J. Virtue[17], H. von der Schmitt[10], J. von Krogh[10], A. Wagner[10], C. Wahl[9], C.P. Ward[5], D.R. Ward[5], J. Waterhouse[6], P.M. Watkins[1], A.T. Watson[1], N.K. Watson[1], M. Weber[10], S. Weisz[7], P.S. Wells[7], N. Wermes[10], M. Weymann[7], G.W. Wilson[19], J.A. Wilson[1], I. Wingerter[7], V-H. Winterer[9], N.C. Wood[13], S. Wotton[7], B. Wuensch[3], T.R. Wyatt[14], R. Yaari[24], Y. Yang[4,b], G. Yekutieli[24], T. Yoshida[22], W. Zeuner[7], G.T. Zorn[15].

[1]School of Physics and Space Research, University of Birmingham, Birmingham, B15 2TT, UK
[2]Dipartimento di Fisica dell' Università di Bologna and INFN, Bologna, 40126, Italy
[3]Physikalisches Institut, Universität Bonn, D-5300 Bonn 1, FRG
[4]Department of Physics, University of California, Riverside, CA 92521 USA
[5]Cavendish Laboratory, Cambridge, CB3 0HE, UK
[6]Carleton University, Dept of Physics, Colonel By Drive, Ottawa, Ontario K1S 5B6, Canada
[7]CERN, European Organisation for Particle Physics, 1211 Geneva 23, Switzerland
[8]Enrico Fermi Institute and Department of Physics, University of Chicago, Chicago Illinois 60637, USA
[9]Fakultät für Physik, Albert Ludwigs Universität, D-7800 Freiburg, FRG
[10]Physikalisches Institut, Universität Heidelberg, Heidelberg, FRG
[11]Queen Mary and Westfield College, University of London, London, E1 4NS, UK
[12]Birkbeck College, London, WC1E 7HV, UK
[13]University College London, London, WC1E 6BT, UK
[14]Department of Physics, Schuster Laboratory, The University, Manchester, M13 9PL, UK
[15]Department of Physics and Astronomy, University of Maryland, College Park, Maryland 20742, USA
[16]Laboratoire de Physique Nucléaire, Université de Montréal, Montréal, Quebec, H3C 3J7, Canada
[17]National Research Council of Canada, Herzberg Institute of Astrophysics, Ottawa, Ontario K1A 0R6, Canada
[18]Rutherford Appleton Laboratory, Chilton, Didcot, Oxfordshire, OX11 0QX, UK
[19]DPhPE, CEN Saclay, F-91191 Gif-sur-Yvette, France
[20]Department of Physics, Technion-Israel Institute of Technology, Haifa 32000, Israel
[21]Department of Physics and Astronomy, Tel Aviv University, Tel Aviv 69978, Israel
[22]International Centre for Elementary Particle Physics and Dept of Physics, University of Tokyo, Tokyo 113, and Kobe University, Kobe 657, Japan
[23]Brunel University, Uxbridge, Middlesex, UB8 3PH UK
[24]Nuclear Physics Department, Weizmann Institute of Science, Rehovot, 76100, Israel

[a]Present address: Dipartimento di Fisica, Università della Calabria, 87036 Rende, Italy
[b]On leave from Harbin Institute of Technology, Harbin, China
[c]Now at Applied Silicon Inc
[d]On leave from Manchester University
[e]On leave from Birmingham University
[f]and TRIUMF, Vancouver, Canada

1 Introduction

Spontaneous Symmetry Breaking is the foundation of the Standard Model of weak and electromagnetic interactions [1]. In local gauge invariant theories, Spontaneous Symmetry Breaking requires the existence of one or more scalar particles, the Higgs boson(s) [2]. However, while the Standard Model has been successful in describing many processes to a high degree of accuracy, these particles have not been observed. In the Minimal Standard Model (MSM), one complex doublet of Higgs fields is introduced, which results in a single scalar Higgs boson (H^0) with a mass which is not specified by the theory. The MSM Higgs boson in the range $3 < m_{H^0} < 19.3\ GeV/c^2$ has already been excluded in an earlier letter [3] by this collaboration; the limit was increased to $25.3\ GeV/c^2$ [4] by searching more data and optimizing the analysis for $m_{H^0} > 2m_b$. The latter analysis is described in detail here, and is used to set limits on MSSM Higgs bosons in the present publication. To date, including the limit presented in this work and earlier publications by this and other experiments using data from the 1989 LEP running, the mass range $0 < m_{H^0} < 25.3\ GeV/c^2$ has been excluded at the 95% confidence level [3,4,5,6,7]. The L3 experiment has increased the upper limit to $32\ GeV/c^2$ [8] using 1990 LEP data.

In the more general case, two Higgs doublets are considered. In this case 6 independent parameters are needed to specify the Higgs sector which contains 5 physical Higgs bosons [9,10]. A popular theory with such a Higgs sector is Supersymmetry (SUSY). In the Minimal SUSY Model (MSSM) one of the Higgs doublets couples to up-type fermions only, while the other couples only to down-type fermions, thereby preventing flavor-changing neutral currents. Of the two neutral scalar Higgs bosons in this model, one (h^0) must be lighter than the Z^0, while the other must be heavier than the Z^0. There is also a charged Higgs pair which has to be heavier than the W-boson, and a neutral CP-odd Higgs boson (A^0) which has to be heavier than the h^0, but can be lighter than the Z^0 and might therefore be accessible to experiments running near the Z^0 resonance. In this model, only two independent parameters are needed to fully specify the Higgs sector. These parameters can be chosen to be:

- $\tan\beta = v_2/v_1$, the ratio of vacuum expectation values of the two Higgs doublets (where doublet 2 couples to up-type quarks and leptons and doublet 1 couples only to down-types)
- m_{h^0}, the mass of the lightest boson.

Alternately, the parameters can be taken as:

- m_{h^0}, the mass of the light scalar Higgs boson
- m_{A^0}, the mass of the CP-odd Higgs boson.

For a given choice of m_{h^0}, m_{A^0} there are two solutions, one for $\tan\beta > 1$ and one for $\tan\beta < 1$. While many models favor $\tan\beta > 1$ [11], the limits obtained in this analysis are presented for both solutions whenever possible.

In the present analysis a search for Higgs bosons was performed using data accumulated during the 1989 scan of the Z^0 resonance; this corresponds to an integrated luminosity of $1.24\ pb^{-1}$ (or about 25,000 reconstructed multihadron events). The energies and integrated luminosities are listed in Table 1. The MSM Higgs boson, as well as the h^0, can be produced in e^+e^- collisions near the Z^0 resonance in association with a virtual Z^{0*} for Higgs boson masses less than the center of mass energy. For the searches presented here, the Higgs boson tends to decay into the most massive particles kinematically possible ($b\bar{b}, c\bar{c}, \tau^+\tau^-$). The decays involving $Z^{0*} \rightarrow (\nu\bar{\nu}\ or\ e^+e^-\ or\ \mu^+\mu^-)$,

have been selected for this study since final states with large missing momentum or isolated lepton pairs are very distinctive. The MSM cross section falls nearly exponentially with increasing Higgs boson mass; for the data sample considered in the present analysis, 3 events would have been produced for a Higgs boson mass of about 45 GeV/c^2. The CP-odd A^0 state cannot be produced in this process, but can be produced together with an h^0 in Z^0 decays, with the cleanest signature found in final states containing a $\tau^+\tau^-$ pair. For nearly equal h^0 and A^0 masses the rate of associated production would be orders of magnitude larger than that for $h^0 Z^{0*}$ production, and therefore the 4 jet final state is useful for searching in the high m_{h^0} region. Various limits on the h^0 and A^0 masses have been published by the Aleph [12] and Delphi [13] experiments.

2 The OPAL detector

The data were recorded at the CERN e^+e^- collider LEP during its 1989 run using the OPAL detector [14], which is a multipurpose apparatus having nearly 4π steradians acceptance. The central detector (CD) consists of a system of tracking chambers inside a 0.435 Tesla solenoidal magnetic volume. The CD system is surrounded by a time-of-flight (TOF) counter array, a lead glass electromagnetic calorimeter (EM) with a presampler, an instrumented magnet return yoke serving as a hadron calorimeter, four layers of outer muon chambers, and an endcap system which includes a low-angle forward detector (FD).

The central tracking detector consists of a precision vertex chamber, a large volume "jet" chamber, and a chamber for tracking in the $r-\theta$ plane (the coordinate system is defined with z along the beam axis, θ and ϕ being the polar and azimuthal angles). The main tracking is done with the jet chamber, a drift chamber of approximately four meter length and two meter radius, with 24 sectors in ϕ and 159 layers of sense-wires in each sector. Tracks having $|\cos\theta| \leq 0.94$ give a minimum of 40 space points in the jet chamber. The time-of-flight system covers the barrel region of $|\cos\theta| \leq 0.82$. It consists of 160 scintillator bars, 6.8 m long and 45 mm thick, located at a radius of 2.4 m.

The electromagnetic calorimeter consists of a cylindrical array of 9440 lead glass blocks of 24.6 radiation lengths thickness covering the range $|\cos\theta| < 0.82$, and 2264 lead glass blocks of 20 radiation lengths thickness in the endcaps covering the region between $0.81 < |\cos\theta| < 0.98$. Each block subtends a solid angle of approximately $40 \times 40\ mrad^2$ and projects towards a point near the interaction point in the barrel region and along the beam direction in the endcaps. The three sections of the electromagnetic calorimeter cover 98% of the solid angle. An "EM cluster" is defined as a group of contiguous lead-glass blocks where each block registers more than 20 MeV.

The luminosity of the colliding beams was determined by observing small angle Bhabha scattering with the Forward Detector, a lead/scintillator calorimeter, with associated tracking chambers, at either end of the central detector with an acceptance covering from $40 < \theta < 150$ mrad and 2π in azimuth. This device achieves a systematic accuracy of 2.2% in the luminosity measurement [15].

The OPAL trigger consists of several independent elements having a high level of redundancy. Of major interest to this analysis are the triggers:

- E_{EM} (summed energy of at least 6 GeV in the lead glass calorimeter)
- TOF (more than 2 adjacent TOF scintillators fire)

- Track Trigger (at least 2 tracks in the event, as defined by a hardware processor).

All three of these triggers are efficient for high-multiplicity events. The track trigger is efficient for events having at least two tracks with $|\cos\theta| < 0.73$, each with a minimum transverse momentum of 450 MeV/c, and having a separation of at least 15° in ϕ, or approximately 0.36 in $\cot\theta$. In the present analysis the track trigger has been demanded, while the other triggers have been used to monitor its efficiency.

The efficiency of the trigger hardware to detect a single isolated track was measured using $e^+e^- \to q\bar{q}$ and $e^+e^- \to e^+e^-$ events, where both processes were triggered by the EM or TOF detectors. The efficiency for single tracks was found to range from 91% for low momentum tracks to 96% for high momentum e^+e^- tracks. The simulation of the OPAL detector response to the generated particles was modelled using the Monte Carlo program GOPAL based on the GEANT [16] package, which provides an accurate description of the response of the various detector components, as demonstrated in references [17,18].

A number of requirements have been imposed for all the data used in this publication. The tracking chamber, forward detector, and electromagnetic calorimeters had to be fully operational, and charged tracks and electromagnetic calorimeter clusters were only considered if they passed certain quality cuts. For charged tracks it was required that:

- $N_{hit} > 40$ (number of hits along a charged track),
- $|d_0| < 2.5\ cm$ (distance of closest approach to the beam axis),
- $|z_0| < 50\ cm$ (the z component of the distance of closest approach to the beam axis),
- $p_T > 0.100\ GeV/c$, and
- $|cos(\theta)| < 0.93$, where θ is the polar angle with respect to the beam axis.

In order to reduce the background from beam gas and beam wall interactions, events with $N_{good}/N_{all} < 0.20$ were removed from the sample, where N_{good} was the number of charged tracks passing the criteria described previously, and N_{all} was the total number of reconstructed charged tracks in the event. For EM clusters it was required that the mimimum cluster energy exceeded 170 MeV in the barrel and 250 MeV in the endcap regions.

3 Minimal Standard Model (MSM) Search

The search for the Minimal Standard Model Higgs boson made use of the decays $Z^0 \to Z^{0*}H^0$, $H^0 \to q\bar{q}$, $Z^{0*} \to (\nu\bar{\nu}\ or\ e^+e^-\ or\ \mu^+\mu^-)$. These decay modes are characterized by either a large missing energy or the presence of two isolated energetic leptons, making them significantly different from multihadron events. In the present search, which addresses the mass range above the $b\bar{b}$ threshold, the Higgs boson decays mainly into pairs of heavy quarks. These final states are characterized by high multiplicity events and consequently more than 5 charged tracks in each event were required.

3.1 Missing Energy Search

The missing energy search was directed towards events of the type $e^+e^- \to Z^{0*}H^0$, $Z^{0*} \to \nu\bar{\nu}$, $H^0 \to q\bar{q}$ which are characterized by a significant momentum imbalance in the event. To

estimate the missing energy/momentum for an event, an algorithm was developed to compute the total 4-momentum of the event from the observed tracks and clusters. First, all EM cluster energies and charged track momenta were summed. A subtraction was then made for each charged track in order to correct for double counting. The amount of energy subtracted was equal to the average energy deposited in the lead glass by charged pions, as a function of their momentum. The accuracy of this algorithm has been shown in reference [3].

After applying the general quality cuts, it was then further required that:

- (A1) $N_{good} > 5$. This cut rejected low-multiplicity events (e.g., dileptons – especially τ pairs, 2-photon events, beam wall events). The cut significantly reduced the acceptance for H^0 masses lower than about 10 GeV/c^2 due to the significant branching fraction for $H^0 \rightarrow \tau^+\tau^-$.
- (A2) $|cos\theta_{thrust}| < 0.9$ and $|cos\theta_{p_{vis}}| < 0.9$. θ_{thrust} is the polar angle of the thrust axis computed using both CD tracks and EM clusters. $\theta_{p_{vis}}$ is the polar angle of the total momentum vector. These cuts removed events having significant energy directed close to the beam direction.
- (A3) $E_{FD} < 2\ GeV$. Events were required to have less than 2 GeV of energy deposited in the forward detector. This cut also rejected events with jets close to the beam, as well as two-photon events.
- (A4) $E_{vis}/E_{cm} < 0.6$. Events were required to have a large missing energy.
- (A5) $p_T > 6\ GeV$. p_T is the transverse momentum measured with respect to the beam axis. The distributions of p_T for the data and the JETSET 7.2 [19] Monte Carlo (MC) for multihadron production are shown in Figure 1. The data is well described by the MC for $p_T > 6\ GeV/c$, while the excess of data at $p_T < 3\ GeV/c$ is mostly due to two-photon events which are not included in the Monte Carlo simulation.
- (A6) $E_{forward}/E_{vis} > 0.7$. The visible energy contained in a cone of full-angle 150° centered about the total visible momentum vector had to be larger than 70% of the total visible energy in the event. In Higgs boson events, the total momentum vector would approximate that of the H^0.
- (A7) $E_{backward} < 2.5\ GeV$. $E_{backward}$ is the visible energy contained in a cone of 120° full-angle, oriented opposite to the total visible momentum direction.

The effects of these cuts both in the data and Monte Carlo (normalized to the luminosity) are shown in Table 2. Detector Monte Carlo simulations demonstrated that, after all the data selection cuts were imposed, the track trigger efficiency was larger than 98% for $m_H > 10\ GeV/c^2$.

Figure 2 is a scatterplot of $E_{forward}/E_{vis}$ versus $E_{backward}$, for the data and for a simulated signal with $m_{H^0} = 24\ GeV/c^2$, after all cuts except A6 and A7. The cut region is also shown in the figure. The population for a Higgs boson signal is seen to be well isolated from the data, and the region defined by cuts A6,A7 contains 85% of the signal remaining after cuts A1-5.

3.2 Dilepton Search

In the search for the decays $Z^0 \rightarrow (e^+e^-\ or\ \mu^+\mu^-)H^0$, the "major" tracks were defined as the two highest-momentum oppositely-charged tracks in the event with an opening-angle larger than 90°. The major tracks also had to be associated with EM clusters registering more than 250 MeV and

had to each have momenta satisfying $p > 10\ GeV/c$, or $p > 5\ GeV/c$ if the associated EM cluster energy was larger than 10 GeV. Clusters were associated with charged tracks if the extrapolation of the track intersected the EM cluster. Roughly speaking, this meant that EM clusters and CD tracks were associated if their directions coincided within 100 mrad.

An isolation condition was then imposed on the major tracks. For each major track, the EM energy within a 30° (half angle) cone around the track was summed. If this energy exceeded the energy of the associated EM cluster by more than 5 GeV, the event was rejected. Also, the scalar momentum sum of any additional tracks in this cone had to be less than 5 GeV/c. Finally, the event had to have at least 4 tracks in addition to the major tracks, separated from them by at least 15°. These cuts had an efficiency exceeding 50% for $m_{H^0} > c\bar{c}$ threshhold; however, no data survived these cuts.

Although there are redundant trigger elements for both the e^+e^- and $\mu^+\mu^-$ channels, the trigger efficiencies have been evaluated using only the track-trigger in a manner similar to that described for the $\nu\bar{\nu}$ channel. For Higgs boson masses above 3 GeV/c^2, the track-trigger efficiency was found to be greater than 98% with a 1% uncertainty after all physics cuts. The probabilities for Higgs boson events to pass the track trigger and the cuts were obtained in the manner described for the analysis of the $\nu\bar{\nu}$ channel, and are summarized in Table 3.

3.3 The Higgs Boson Generators

The Higgs boson cross section was calculated using the Berends and Kleiss Born generator [20] which incorporates first order QED corrections, and using the improved Born approximation (IBA) [21] with the value $m_Z = 91.15\ GeV/c^2$ and the corresponding Standard Model value for Γ_Z, while taking into account the effective electro-weak couplings $\alpha(Q^2)$ and $sin^2\theta_W$ at the Z^0 mass. The IBA tends to increase the cross section for heavier top masses (m_t) by a factor $(1 + 3\Delta\rho)$, where $\Delta\rho = 3G_F m_t^2/8\sqrt{2}\pi^2$. However, an additional contribution, unique to Higgs boson production, arises from a top quark triangle graph at the ZZH vertex. This diagram reduces the cross section by a factor $(1 - \frac{8}{3}\Delta\rho)$ [22]. Consequently, the dependence of the cross section on m_t is negligible.

The effect of initial state radiation was calculated using the exponentiation technique. Both the Berends, Burgers and van Neerven calculations [23] and the results of Nicrosini and Trentadue [24] have been studied. The two methods give results which differ by less than 0.5%.

Based on a study of the dependence of the cross section on the relevant parameters, a conservative uncertainty of 5% on the cross section formalism has been estimated. For example, the cross section changes less than 0.4% for a $\pm 100\ MeV$ change in the Z^0 mass, and the effect of the top quark triangle graph is less than 3% when $m_t \leq 200\ GeV/c^2$.

The energy dependence of the Higgs boson production cross section was taken into account since the data were taken at several center-of-mass energies. The effect on the acceptance of scanning across the Z^0 peak was found to be negligible.

3.4 Systematic Uncertainties and Mass Limit

The systematic uncertainties due to the modelling of the acceptance arise primarily from fragmentation modelling and energy measurement in the detector. The final-state quark fragmentation

has been modelled with the LUND (JETSET 6.3) shower Monte Carlo. Since the b-quarks from the Higgs boson decay have a hard fragmentation, the main uncertainty is associated with the knowledge of B meson decay properties. The only selection requirement which is sensitive to this issue is that based on the charged-track multiplicity. Varying the multiplicity cut by 1 unit leads to a 4% change in the acceptance, which has been considered as the overall systematic uncertainty due to fragmentation.

The uncertainty due to the detector energy response has been estimated by comparing the acceptance calculated using two simulations which differ in their modelling of the calorimeter response. Differences of as much as 3% in the acceptance have been realized in this study; thus, a conservative systematic uncertainty of 4% has been used.

The uncertainty on the track trigger efficiency is estimated to be 1% in this high-multiplicity analysis. Adding all of the uncertainties in quadrature, with 2.2% for luminosity and 5% for the cross section calculation, one obtains a total systematic uncertainty of 7.9%.

The numbers of expected Higgs bosons, as a function of m_{H^0}, are listed in Table 3. Figure 3 shows the expected numbers of events, reduced by the 8% systematic uncertainty; the range $3 < m_{H^0} < 25.3\ GeV/c^2$ is ruled out at the 95% confidence level.

4 Minimal Supersymmetric Model (MSSM) Searches

The minimal SUSY model has at least one Higgs boson with a mass below that of the Z^0 which would be produced in LEP running near the Z^0 resonance. The lightest MSSM Higgs boson is a scalar denoted by h^0; there also exists in this model a CP-odd state (often referred to as a "pseudoscalar") denoted by A^0, which can be lighter than the Z^0. The search for MSM Higgs bosons described in the previous section can be applied directly to the mode $Z^0 \rightarrow Z^{0*}h^0$ to exclude a significant region of the m_{h^0}, m_{A^0} parameter space. Other regions of the parameter space have been excluded using the decay $Z^0 \rightarrow h^0A^0$, where the Higgs bosons could be identified by their decays into $c\bar{c}$, $b\bar{b}$, and $\tau^+\tau^-$. These processes must be examined separately for the assumptions $\tan\beta > 1$ (i.e., $h^0, A^0 \rightarrow b\bar{b}, \tau^+\tau^-$ mostly), and $\tan\beta < 1$ (i.e., $h^0, A^0 \rightarrow c\bar{c}$ mostly, with $\tau^+\tau^-$ final states suppressed.)

The m_{h^0}, m_{A^0} parameter space is shown in Figure 4, which indicates the limits obtained from the analyses to be described subsequently; only the region $m_{A^0} > m_{h^0}$ is of interest due to a constraint in the model. There is potentially copious h^0, A^0 production on the $m_{h^0} = m_{A^0}$ diagonal which decreases for increasing m_{h^0} and as the distance from the diagonal increases. Searches using the 4 jet final state are efficient for higher values of m_{h^0} (curve D in the figure), while the $\tau^+\tau^-$ *jet jet* topology has a good efficiency down to low values of m_{h^0} (curves C-L and C-H), but is sensitive only for $\tan\beta > 1$. The 4 τ final state can be used to cover the m_{h^0} region between charm and bottom threshold, again only for $\tan\beta > 1$ (region E). The region far from the diagonal has a small production rate for h^0A^0, but can be excluded by using the h^0Z^{0*} channel (the region enclosed by curve B in Figure 4).

In calculating the production cross sections, the various center of mass energies were taken into account, and all the corrections used in the MSM analysis were included, except for those involving top quark and heavy SUSY particle loops.

4.1 $Z^0 \to Z^{0*}h^0$

The limit on $\Gamma(Z^0 \to H^0 Z^{0*})$ obtained for the MSM can also be interpreted as a limit on $\Gamma(Z^0 \to h^0 Z^{0*})$, and so can be used to restrict the masses of the bosons h^0 and A^0 from the relation:

$$\Gamma(Z^0 \to h^0 Z^{0*}) \;=\; sin^2(\beta - \alpha) \times \Gamma(Z^0 \to H^0 Z^{0*}) \qquad (1)$$

where α is the Higgs boson mixing angle [10]. Withing the framework of the MSSM, α and β are related to m_{h^0} and m_{A^0} by the requirements of supersymmetry. The excluded region obtained in this manner is shown in Figure 4 as curve B. For m_{h^0} below the $b\bar{b}$ threshold (and $\tan\beta > 1$) the lower-mass MSM analysis has been used [3] since it is less sensitive to the relative amount of $h^0 \to \tau^+\tau^-$ decays, while for larger masses the MSM analysis presented in this paper was used. This accounts for the discontinuity in the limit curve at the $b\bar{b}$ threshold.

For the case $\tan\beta < 1$, the dominant decay mode of h^0 is into $c\bar{c}$, with a rather small fraction going into $b\bar{b}$. Especially for the higher mass region, the $c\bar{c}$ mode has a topology with a greater confinment of the jet energy in the forward direction. The acceptance for this mode has been modelled with JETSET 6.3, and it was found to be comparable to the acceptance of the $b\bar{b}$ mode within the MC statistics. Consequently, the excluded region is valid for all values of $\tan\beta$, and the analysis can be applied directly to more general classes of models in which the Higgs bosons are expected to decay primarily into $b\bar{b}$ and $c\bar{c}$.

4.2 $Z^0 \to h^0 A^0 \to \tau^+\tau^-\tau^+\tau^-$

4.2.1 Analysis Procedure

In the mass region above the charmonium resonances, and for $\tan\beta > 1$, the minimal SUSY model predicts an enhancement of the decay into $\tau^+\tau^-$ relative to that into $c\bar{c}$. This allows one to look for Higgs pair production through the 4 τ decay channel which results in a four-prong final state 55% of the time. The search for this channel required a 4-prong final state with kinematics consistent with that of h^0A^0 production.

Events passed an initial pre-selection if:

- Exactly 4 tracks were found.
- The scalar sum of track momenta exceeded $E_{beam}/2$.
- Less than 2 GeV of energy was deposited in the forward detector.

Events passing this pre-selection procedure were then subjected to further cuts:

- (B1) $|cos(\theta_{thrust})| < 0.7$. The thrust axis was calculated using only charged tracks. This cut retained only events well within the track trigger acceptance.
- (B2) $p_{track} > 0.2\ GeV/c$. This supressed events with photon conversions.
- (B3) $E_{EM} < 80\ GeV$. This cut on the total visible EM energy rejected Bhabha and $e^+e^- \to \gamma\gamma$ events with converting photons.

- (B4) $M_{pair} < 15\ GeV/c^2$. The four tracks in the event can be paired in three ways. In at least one of the three configurations, the invariant masses of both of the track pairs had to satisfy the cut. This cut emphasized a topology for a pair of Higgs bosons with masses below 10 GeV/c^2.

- (B5) $M_{T3} > 2.5\ GeV/c^2$. The three-track transverse mass had to be larger than the value realised for $\tau^+\tau^-$ events of the 1+3 track topology for all possible 3-track combinations in the event. While this cut eliminated mostly $\tau^+\tau^-$ events, it also rejected lepton pair events with a converting photon that were not rejected by the previous cuts.

No events survived the above requirements.

4.2.2 Systematic Uncertainties and Mass Limits

The signal selection efficiency was found to be higher than 22% in region E of Figure 4. Backgrounds were simulated using KORALZ37 [26] for lepton pairs and HERWIG34 [27] for QCD events; the simulation predicts one τ-pair event expected in the data. The systematic error for these procedures was conservatively estimated to be 7% based on the Monte Carlo statistics and the modelling of tracking and EM energy response in the detector. Table 4 summarizes the number of events analysed and the number of events passing each stage of the analysis.

Summing the luminosity and selection uncertainties in quadrature, one gets a total systematic error of 7.4%. The expected number of observed events was calculated taking into account the branching ratio, the selection efficiency, and the trigger efficiency. The contour in the m_{h^0}, m_{A^0} plane where one expects to observe more than 5 events is given by region E in Figure 4. Note that region E is bounded from above and from the right by the $b\bar{b}$ threshold, at which the $\tau^+\tau^-$ branching ratios of the Higgs bosons are unknown due to possible mixing with bound states of the $b\bar{b}$ system (χ_b), as discussed in the next section.

4.3 $Z^0 \rightarrow h^0 A^0 \rightarrow \tau^+\tau^-\ jet\ jet$

4.3.1 Analysis Procedure

For $\tan\beta > 1$ and masses above the $b\bar{b}$ threshold, the h^0 and A^0 are expected to decay primarily into b-quarks. The decay into a pair of τ leptons, which has a distinct signature, is enhanced by QCD corrections and has a branching ratio of 6% to 8%. However, this is not necessarily the case in region F of Figure 4, where the h^0 or A^0 can mix with χ_b states since their widths are expected to be comparable. The present analysis is restricted to the case in which the two τ leptons decay into a single charged track each; this decay mode leads to a distinct final state which consists of two isolated charged tracks recoiling against a heavy hadronic system. The 3-prong decay mode of the τ has not been used since it contains a large background from multihadronic decays of the Z^0.

Events had to pass an initial pre-selection requiring that at least 8 good charged tracks were found. A simple algorithm was then applied to search for events having a τ-pair candidate with each τ decaying into a single track. Pairs of oppositely charged tracks which were isolated from the rest of the event were identified as $\tau^+\tau^-$ candidates if:

- Each of the two charged tracks had a momentum in excess of 1 GeV/c.

- Each of the tracks was isolated from all other charged tracks (excluding the other track of the pair) by more than 30°.
- The pair direction (vector sum of the two track momenta) had to be isolated by 30° from all tracks, excluding the tracks comprising the pair.

If multiple pairs were identified in an event, only the highest energy pair was retained. These cuts identified such pairs in 1886 events.

It has not been possible to devise a single set of cuts with high efficiency over the entire range of scalar Higgs boson masses since the τ-pair and b-jets assume rather different topologies for light and heavy Higgs boson masses. The analysis presented here makes use of two sets of cuts, one being efficient for m_h-m_A near $b\bar{b}$ threshold and starting to lose efficiency for $m_h > 20\ GeV/c^2$. The other analysis has a superior efficiency for $m_h > 20\ GeV/c^2$.

4.3.2 Higher-mass Analysis

The Higgs bosons are pair produced, carrying approximately half of the c.m. energy each. This results in the τ decay products having a hard energy spectrum compared to the hadronic background. Furthermore, the energetic τ-leptons in signal events would give a large missing energy directed along the reconstructed $\tau^+\tau^-$ pair (Higgs boson) direction.

Due to the back-to-back configuration of the two Higgs bosons, the two τ leptons coming from one of them will generally be isolated from the rest of the event. Therefore, no additional EM energy (i.e. energy not associated with the two τ leptons) should be deposited in the EM calorimeter in a region about the $\tau\tau$ pair. Studies of $\tau\tau$ data and MC events demonstrate that electromagnetic energy associated with the τ leptons is almost entirely confined to the two cones of 18° half angle about each of the tracks; this EM energy is not included when summing the unassociated energy.

The topology cuts for this part of the analysis were:

- (C1H) $E_{pair} > 4.55\ GeV$. The scalar sum of the momenta of the tracks comprising the pair had to be larger than 10% of the nominal beam energy. The E_{pair} distibution is shown in Figure 5.
- (C2H) $E_{cone} < 2\ GeV$. Events with more than 2 GeV of unassociated energy in a cone of 73° half angle ($\cos\theta = 0.3$) about the pair direction were rejected. The distribution of the unassociated energy is shown in Figure 6.
- (C3H) $\cos\theta_{pair-p(total)} < 0.8$. $\theta_{pair-p(total)}$ is the angle between the pair direction and the total observed momentum of the event. This distribution is shown in Figure 7.

After employing these kinematical restrictions, the remaining background primarily consisted of two jet events. The sphericity of such events is small, while the signal, having a τ pair and two b-jets, has a moderately large sphericity even for light Higgs bosons. The additional requirements imposed were:

- (C4H) $Sphericity > 0.1$. The sphericity distribution is shown in Figure 8.
- (C5H) $cos(\theta_{open}) < 0.6$. θ_{open} is the opening angle between the two pair tracks. In jets this angle is peaked near unity, while the signal has a finite minimal opening angle (even for light Higgs bosons); this is shown in Figure 9.

No event survived these cuts.

The cuts and their effect on both the data and an example of a signal are give in Table 5. The signal selection efficiency varied between about 35% (for $m_{h^0} = 25$, $m_{A^0} = 35\ GeV/c^2$) to about 15% ($m_{h^0} = 40$, $m_{A^0} = 40\ GeV/c^2$). The sphericity cut prevented extending this analysis to the low mass region, and the correlation requirement between the $\tau\tau$ direction and the total momentum, as well as the isolation requirements, makes these cuts inadequate for heavier masses.

4.3.3 Lower-mass Analysis

The topology of the mass range $m_{h^0} = 5 - 20\ GeV/c^2$ is similar to the one which characterizes the heavier Higgs boson case. Basically the same analysis was followed, but the value of the cuts had to be modified to suit the different kinematical region.

- (C1L) $E_{pair} > 9.1\ GeV$. This value represents 20% of the mean beam energy.
- (C2L) $E_{cone} < 2\ GeV$. The cone comprised the entire hemisphere about the pair direction.
- (C3L) $N_{track}^{hemi} = 2$. It was required that no tracks apart from those comprising the pair be found in this hemisphere.
- (C4L) $cos(\theta_{open}) < 0.95$.
- (C5L) $\cos\theta_{pair-p(total)} < 0.8$.
- (C6L) $Sphericity > 0.04$.

No events passed these cuts. The cuts and their effect on both the data and an example of a signal are give in Table 6. The signal selection efficiency varied between about 30% (for $m_{h^0} = 15$, $m_{A^0} = 25\ GeV/c^2$) to about 10% ($m_{h^0} = 8$, $m_{A^0} = 11\ GeV/c^2$).

4.3.4 Sytematic Uncertainties and Mass Limits

QCD corrections to the decay of the Higgs into a $q\bar{q}$ system were taken into account according to the formalism given in reference [25], and the corrected branching ratios for both $b\bar{b}$ and $\tau^+\tau^-$ have been used. Systematic uncertainies on the modelling of the signal arise from the production cross section, the measured luminosity, the detector response (GOPAL), and the modelling of fragmentation in the JETSET generator. The uncertainty on detector modelling (9%) has been conservatively estimated from the MC statistical errors (3%), comparisons of several versions of the OPAL dectector simulation program (5%), and by varying the cuts by somewhat more than the resolution on the measured quantity (7%). The multiplicity cut is somewhat sensitive to the B decay model used in JETSET 6.3, and a 4% uncertainty has been included for fragmentation effects, as described in the MSM analysis. These sources result in a total systematic uncertainty of 10%, which is used to scale down the generated signal in order to obtain the 95% C. L. limits on the h,A masses.

The resulting limits are indicated in Figure 4 as curves C. Special attention should be given to the low mass region, since when one of the Higgs boson masses overlaps with the χ_b resonance states (9.5-11 GeV), the branching ratio is completely unknown. At the low-m_h end of contour C-L in Figure 4, one of the Higgs bosons is in the resonance region, and its branching ratio has been conservatively assumed to be 100% to multihadrons, which results in a reduced sensitivity.

4.4 $Z^0 \rightarrow h^0 A^0 \rightarrow 4\ jets$

4.4.1 Analysis Procedure

For Higgs boson masses larger than the $b\bar{b}$ threshold, and for $\tan\beta > 1$, the predominant decay modes of the h^0 and A^0 are into $b\bar{b}$ pairs, with branching ratios in the vicinity of 93 %. For Higgs bosons with masses larger than about 20 GeV/c^2 the events are rather spherical, thus event shape variables such as thrust and acoplanarity provide a convenient means to distinguish the Higgs boson signal from the QCD background. Also, the underlying 4-jet structure with four identical b-quark jets can be used to differentiate between the signal and the background. Although individual b-jets cannot be differentiated from other jets with a high efficiency by using the apparent jet mass, the average mass of the four b-jets is noticeably different from that obtained for the QCD background.

Jets were defined by applying the JADE clustering algorithm [28] to the events, including both tracks and EM clusters. The jet resolution parameter ($ycut = 0.03$) was chosen to maximize, within the sample of 4-jet events, the product of the signal efficiency and the signal-to-background ratio. The jet four-momenta were corrected for double counting of charged particle energy using the energy algorithm described earlier.

After applying the track and cluster quality cuts listed in section 2, the following requirements were imposed:

- (D1) $Thrust < 0.85$. The thrust of the event was calculated using both charged tracks and EM clusters.
- (D2) $N_{jet} = 4$. Exactly four jets were required in the event. Each of the four jets was required to have at least 3 tracks or clusters, to have an energy larger than 5 GeV, and to form an angle θ with the beam axis satisfying $|\cos\theta| < 0.9$.
- (D3) $\bar{M} < 7.5\ GeV/c^2$, $\bar{D} < 5.0\ GeV/c^2$. The average of the four jet masses is denoted by $\overline{M} = (\Sigma M_j)/4$, and $\overline{D} = (\Sigma \mid M_j - M_i \mid)/6$ is the average of the six mass differences. Figures 10,11 show the distributions of these quantities for the data, for a Monte Carlo simulation of the QCD background, and for a hypothetical Higgs boson signal.
- (D4) Kinematics. The four jets in each event can be combined into pairs in three different ways. For at least one of the three possible configurations it was required that both jet pairs satisfy the following kinematical requirements:
  - (1) the combined jet-jet momenta had to be larger than 18 GeV/c (for comparison, if the Higgs boson masses are both 40 GeV/c^2, their momenta are 22 GeV/c);
  - (2) the ratio of the two jet-jet momenta had to lie between 0.7 and 1.3;
  - (3) the directions of the two jet-jet momenta with respect to the beam direction had to satisfy $|\cos\theta| < 0.5$;
  - (4) the two jet-jet decay angles δ in their own rest frame (the angles between the jet-jet directions and the pair-boost) had to satisfy $|\cos\delta| < 0.7$.

  Condition (2) eliminates events which are incompletely contained in the detector; such events are usually at extreme polar angles and have a visible energy which is low compared to that for fully contained events. Condition (3) uses the difference between the production angular distributions of the Higgs boson signal [$\sim \sin^2\theta$] and the QCD background [$\sim (1 + \cos^2\theta)$]. Condition (4) uses the fact that the Higgs boson decay is random with respect to

the boost direction, while in the case of the QCD background the gluon radiation is emitted preferentially along the direction of the quark (along the boost).

- (D5) *Acoplanarity(tracks)* > 0.16, *Acoplanarity(clusters)* > 0.20. Acoplanarity is defined as $4 \times (\sum |P_{i,\perp}| / \sum |P_i|)^2$, where $P_{i,\perp}$ is the momentum or energy component of particle i with respect to the axis which minimizes the $\sum |P_{i,\perp}|$. The acoplanarity distributions, as obtained using tracks and clusters separately, are shown in Figures 12,13.

The effect of the cuts on the data, the simulated QCD background, and on a hypothetical Higgs boson signal are listed in Table 7. There were 10 events in the data which passed these cuts, whereas the QCD Monte Carlo predicts 13.3 events. The efficiency for a Higgs boson signal with $m_{h^0} = 35$, $m_{A^0} = 40\ GeV/c^2$ is 9.4% (see Table 7).

4.4.2 Systematic Uncertainties and Mass Limits

The quantities on which the present analysis is based (global shape variables and jet rates) do not depend critically on details of the detector performance [18,29]. The main systematic errors arise from theoretical uncertainties in the modelling of gluon radiation and of quark and gluon fragmentation. In a previous publication it was demonstrated [17] that the global properties of multihadron events measured by OPAL are adequately described by currently used Monte Carlo programs such as JETSET 7.2 and HERWIG 3.4. To assess the effect of possible uncertainties from fragmentation on the results of the present analysis, various simulations of the QCD background were compared to the data. First, the JETSET and HERWIG generators were compared using the set of parameters which resulted from the optimization procedure of reference [17]. Then some of the parameters of JETSET most relevant to fragmentation and gluon radiation were varied over ranges compatible with OPAL data.

The stability of the acceptance with regards to the Monte Carlo simulation is shown in Tables 8 and 9 which list the efficiency of the individual selection cuts for the data and for the various Monte Carlo samples used in this study. The four "special" samples of the JETSET 7.2 Monte Carlo were obtained by varying the values of Λ_{QCD} $[GeV]$ and σ_q $[GeV/c]$, within the ranges 0.27-0.31 and 0.33-0.41, respectively; these parameters govern the longitudinal and transverse properties of quark and gluon jets and the amount of gluon radiation. Samples "sp.1" to "sp.4" correspond to $(\Lambda_{QCD}, \sigma_q) = (0.27,0.37)$, $(0.31,0.37)$, $(0.29,0.33)$ and $(0.29,0.41)$ respectively (see Table 2 in ref. [17]).

The last rows of Tables 8 and 9 list the mean selection efficiencies ($\bar{\epsilon}$) averaged over the various MC samples, and also their r.m.s. scatter about the mean. These scatters were used to estimate a global systematic uncertainty of $\pm 13\%$ on the residual background. This is combined with the statistical error of 20% to give a total error on the background of 24%.

In the case of the Higgs boson signal, similar studies have been carried out using JETSET 6.3. The systematic errors on the signal efficiency due to the various cuts were evaluated to be 5% for shape-variable cuts, 3% for the 4-jet requirements, and 4% for the kinematics cuts. Cut (D3), which is based on the effective mass of the four b-jets, has been studied with special emphasis on b-quark fragmentation. While the r.m.s. width of the $\overline{M}$ and $\overline{D}$ distributions and the mean value of $\overline{D}$ show no significant variations, the mean value of $\overline{M}$ changed somewhat when the hardness of the b fragmentation function was varied. The b-quarks fragment at an energy equal to the Higgs boson mass, which is in the vicinity of 35 GeV in the present search . At such energies b-quark fragmentation is well known from measurements at PETRA and PEP. In particular, the

$z = (E+p)_{B-meson}/(E+p)_{quark}$ distribution was found [30] to have a mean value $< z >$ of 0.835 ± 0.035 (world average). To study the dependence of $\overline{M}$ on b-quark fragmentation, the Petersen fragmentation function (see e.g. reference [30]) was used and the value of ϵ_b was varied. It was found that the experimental range of $< z >$ was covered for ϵ_b varying between 0.005 and 0.020. The corresponding variation of the mean value of $\overline{M}$ (6.7 to 7.1) translates into a systematic uncertainty of ± 5 % on the Higgs boson signal efficiency. A value $\epsilon_b = 0.01$ was adopted for the simulations of the Higgs boson signal. It was also verified that the $\overline{M}$ and $\overline{D}$ distributions were insensitive to the choice of the Higgs boson masses.

Adding in quadrature all systematic errors in efficiency, one obtains $\pm 9\%$, which is comparable to the statistical error (10%); the combined error on the Higgs boson signal efficiencies is thus 14%. The 95% C.L. limit on a signal for 10 observed events and a calculated background of 13.3 ± 3.2 is 7.8 events. The formalism recommended by the Particle Data Group [31] was used to obtain this number; the background was conservatively estimated to be 13.3 - 3.2 = 10.1 events. The excluded region in the m_{h^0},m_{A^0} plane is shown as curve D in Figure 4.

For $\tan\beta < 1$, the dominant decay modes of both h^0 and A^0 are into $c\bar{c}$, with only a fraction (< 20 %) going into $b\bar{b}$ (this fraction is zero if the two Higgs boson masses are equal). Also, for a given m_{h^0}, m_{A^0} the production cross sections are the same for $\tan\beta < 1$ and $\tan\beta > 1$. The selection criteria are to a large extent independent of the quark flavour with the exception of selection (D3) which is based on the average jet mass and average mass difference. Therefore, the $\overline{M}$ and $\overline{D}$ distributions were studied for the case of a $4c$-quark final state. The JETSET 6.3 Monte Carlo was again used, with $\Lambda_{QCD} = 0.29$ and $\sigma_q = 0.37$. Charm fragmentation effects were studied using the Petersen function with ϵ_c varied over a wide range. For each value of ϵ_c the z_c distribution was compared to the distribution measured at PETRA and PEP for 29-35 GeV c.m.s. energy. These measurements span the range $< z_c >= 0.68 \pm 0.04$ [30], which is covered by a variation of the parameter ϵ in the Petersen function of $0.04 < \epsilon_c < 0.13$. For this range of ϵ_c, the mean of $\overline{M}$ varied from 5.17 to 5.44 and the mean of $\overline{D}$ from 3.08 to 3.18. These values are considerably *lower* than what was found in the case of $4b$-quark final states, thus leading to a more efficient separation from the background. Keeping all selection criteria unchanged, one obtains a selection efficiency which is about 10 % higher in the $4c$ case than in the $4b$ case. A higher efficiency was also obtained for a *mixed* sample where one of the Higgs particles was required to decay into $c\bar{c}$ and the other into $b\bar{b}$. Thus, one can conservatively claim that the limits obtained in this section apply both for $\tan\beta > 1$ and $\tan\beta < 1$.

5 Conclusions

An analysis has been presented which excludes the existence of a minimal Standard Model Higgs boson in the mass range of $3.0 < m_{H^0} < 25.3\ GeV/c^2$ at the 95% confidence level. The null result from this analysis has also been used to set limits on the lowest-mass MSSM Higgs boson via the channel $Z^0 \rightarrow h^0 Z^{0*}$. As the present analysis is equally sensitive to h^0 decays into $b\bar{b}$ and $c\bar{c}$ final states, the limits on m_{h^0} hold for both $\tan\beta > 1$ and $\tan\beta < 1$. The excluded range of m_{h^0}, m_{A^0} is delimited by curve B in Figure 4, or alternately by curve B in Figure 14 which is plotted in the m_{h^0}, $\tan\beta$ parameter space.

The limits on MSSM Higgs bosons have been significantly extended by searching for the decays $Z^0 \rightarrow h^0 A^0$, where the Higgs bosons decay either into heavy quarks or $\tau^+\tau^-$. The $\tau^+\tau^-$ *jet jet* final state has a clean signature over a wide mass range, but is sensitive mostly for $\tan\beta > 1$. On the other hand, the higher mass limits obtained from the searches for the 4-jet final state

hold both for $\tan\beta > 1$ and $\tan\beta < 1$. The regions excluded by these channels are indicated by curves C, D and E in Figures 4 and 14. For the theoretically favored case of $\tan\beta > 1$ the range $3 < [m_{h^0}\ and\ m_{A^0}] < 40.5\ GeV/c^2$ is excluded at the 95% confidence level. It is worth noting that some of the searches performed in this analysis are limited by the available statistics and therefore the range of Higgs boson masses for which these analyses are sensitive will continue to expand as this experiment accumulates more data.

6 Acknowledgments

It is a pleasure to thank the SL Division for continuing close cooperation with our experimental group. The assistance of W. Hollik in understanding the cross section calculations is gratefully acknowledged. In addition to the support staff at the participating institutions, it is a pleasure to acknowledge the following: The Bundesministerium für Forschung und Technologie, FRG, The Department of Energy, USA, The Institut de Recherche Fondamentale du Commissariat a l'Energie Atomique, The Israeli Ministry of Science, The Minerva Gesellschaft, The U.S.A.-Israel Binational Science Foundation, The National Science Foundation, USA, The Natural Sciences and Engineering Research Council, Canada, The Japanese Ministry of Education, Science and Culture (the Monbusho) and a grant under the Monbusho International Science Research Program, The Science and Engineering Research Council, UK and The A. P. Sloan Foundation.

References

[1] S. L. Glashow, J. Iliopoulos and L. Maiani, Phys. Rev. **D2** (1970) 1285 ; S. Weinberg, Phys. Rev. Lett. **19** (1967) 1264; A. Salam, *Elementary Particle Theory*, ed. N. Svartholm (Almquist and Wiksells, Stockholm, 1969), p. 367.

[2] P. W. Higgs, Phys. Lett. **12** (1964) 132; F. Englert and R. Brout, Phys. Rev. Lett. **13** (1964) 321; G. S. Guralnik, C. R. Hagen, and T. W. B. Kibble, Phys. Rev. Lett. **13** (1964) 585.

[3] M. Z. Akrawy *et al.*, Phys. Lett. **B236** (1990) 224.

[4] D. Lellouch, *Searches for New Particles with the OPAL Detector*, XX Rencontre de Moriond, Les Arcs, France (1990).

[5] D. Decamp *et al.*, Phys. Lett. **B236** (1990) 233; D. Decamp *et al.*, Phys. Lett. **B241** (1990) 141.

[6] P. Abreu *et al.*, CERN-EP/90-44 (1990).

[7] D. Decamp *et al.*, CERN EP/90-70 (1990).

[8] B. Adeva *et al.*, L3 preprint 10 (1990).

[9] P. J. Franzini and P. Taxil (conveners), *Higgs Search* in CERN 89-08, V. 2, p. 59 (1989);

[10] S. Dawson, J. F. Gunion, H. E. Haber and G. L. Kane, *The Higgs Hunter's Guide*, BNL-41644 (1989), submitted to Phys. Rep..

[11] J. L. Lopez and D. V. Nanopoulos, CTP-TAMU-14/90 (1990).

[12] D. Decamp *et al.*, Phys. Lett. **B237** (1990) 291.

[13] P. Abreu *et al.*, CERN-EP/90-60 (1990).

[14] OPAL Technical Proposal (1983) and CERN/LEPC/83-4.

[15] M. Z. Akrawy *et al.*, Phys. Lett. **B240** (1990) 497.

[16] R. Brun, F. Bruyant, M. Maire, A. C. McPherson and P. Zanarini, *GEANT3*, CERN DD/EE/84-1 (1987).

[17] M. Z. Akrawy *et al.*, CERN-EP/90-48 (1990) (submitted to Zeit. Phys. C).

[18] M. Z. Akrawy *et al.*, Phys. Lett. B236 (1990) 364.

[19] M. Bengtsson and T. Sjostrand, Nucl. Phys. **B289** (1987) 810.

[20] F.A. Berends and R. Kleiss, Nucl. Phys. **B260** (1985) 32.

[21] M. Consoli and W. Hollik,*Electroweak Corrections for Z Physics*, in CERN 89-8, V. 1, p. 39.

[22] Z. Hioki, Phys. Lett. **B224** (1989) 417.

[23] F.A. Berends, G. Burgers and W.L. van Neerven, Nucl. Phys. **B297** (1988) 429.

[24] O. Nicrosini and L. Trentadue, Phys. Lett. **B196** (1987) 551.

[25] E. Braaten and J. P. Leveille, Phys. Rev. **D22** (1980) 715; N. Sakai, Phys. Rev. **D22** (1980) 2220; T. Inami and T. Kubota, Nucl. Phys. **B179** (1981) 171.

[26] S. Jadach, B. F. L. Ward, Z. Was, R. G. S. Stuart, and W. Hollik, *KORALZ the Monte Carlo Program for τ and μ pair Production Processes at LEP/SLC*, unpublished (1989).

[27] G. Marchesini and B. R. Webber, Nucl. Phys. **B310** (1988) 461.

[28] W. Bartel *et al.*, Z. Phys. **C33** (1986) 23.

[29] M. Z. Akrawy *et al.*, Phys. Lett. **B235** (1990) 389.

[30] J. Chrin, Annals New York Acad. Sci. 535 (1988) 131.

[31] G.P. Yost *et al.*, Phys. Lett. **B204** (1988) 4.

Tables

Table 1: Center of mass energies and integrated luminosity for the data in this analysis. N_H are the predicted numbers of Higgs bosons produced via $Z^0 \rightarrow Z^{0*}H^0$, for all decay channels of the Z^{0*} and H^0, with an assumed top mass of 100 GeV/c^2. The systematic error on the luminosity is 2.2%.

E_{cm} (GeV)	$\int \mathcal{L}dt$ (nb^{-1})	N_H, $m_H =$ 24 GeV/c^2
88.264	16	0.10
88.284	125	0.39
89.282	54	0.34
90.260	19	0.28
90.270	6	0.09
90.284	90	1.34
91.000	24	0.56
91.034	150	3.62
91.252	22	0.56
91.268	48	1.20
91.282	148	3.75
91.534	211	5.23
92.250	11	0.21
92.288	59	1.08
92.520	12	0.19
93.248	19	0.22
93.260	28	0.31
93.272	5	0.06
93.284	84	0.93
94.284	94	0.69
95.032	17	0.10

Table 2: Effects of the cuts for the $\nu\bar{\nu}$ search channel. The cuts are described in detail in the text. The MC events are normalized to 1.24 pb^{-1}; for cuts 1-6 the data include beam gas and two photon events which are not included in the Monte Carlo modelling.

Cut	Data	H^0 of mass 24 GeV/c^2
A1) $N_{trk} > 5$	23726	90%
A2) $\lvert\cos(\theta_{thrust})\rvert, \lvert\cos(\theta_{p_{vis}})\rvert \leq 0.9$	19667	83%
A3) $E_{FD} \leq 2.0\ GeV$	19452	82%
A4) $E_{vis}/E_{cm} < 0.6$	762	82%
A5) $P_T > 6\ GeV$	357	76%
A6) $E_{forward}/E_{vis} > 0.7$	110	72%
A7) $E_{backward} < 2.5\ GeV$	0	65%

Table 3: Number of predicted events in the missing energy and dilepton MSM search channels, for various Higgs boson masses. The efficiency (ϵ) shown is the total experimental acceptance and detection efficiency. N_{ff} is the expected number of observed events after all cuts, and l^+l^- refers to e^+e^- and $\mu^+\mu^-$. A top mass of 100 GeV/c^2 has been used for the estimates.

m_H (GeV/c^2)	$\epsilon(\nu\bar{\nu})$	$N_{\nu\bar{\nu}}$	$\epsilon(l^+l^-)$	$N_{l^+l^-}$
3	0.06	2.61	0.36	5.33
5	0.20	6.09	0.50	5.18
7	0.33	7.61	0.60	4.71
10	0.48	7.80	0.64	3.54
12	0.60	7.91	0.66	2.96
14	0.69	7.46	0.67	2.46
16	0.72	6.42	0.66	2.00
18	0.71	5.26	0.66	1.66
20	0.67	4.15	0.65	1.37
22	0.66	3.41	0.65	1.14
24	0.65	2.81	0.63	0.93
26	0.61	2.20	0.62	0.76
28	0.55	1.66	0.62	0.63

Table 4: Signal selection efficiency and background rejection for the $h^0, A^0 \to 4\tau$ analysis.

Cut	Signal MC $m_h = 5, m_A = 7\ GeV/c^2$	$\tau^+\tau^-$ MC	QCD MC	Data
Generated	161	5000	5000	294165
Preselection	49	947	2	340
B1) $\lvert cos(\theta_{thrust})\rvert < 0.7$	36	699	0	204
B2) $p_{track} > 0.2\ GeV/c$	36	692	0	200
B3) $E_{EM} < 80\ GeV$	36	692	0	179
B4) $M_{pair} < 15\ GeV/c^2$	36	405	0	123
B5) $M_{T3} > 2.5\ GeV/c^2$	36	5	0	0
efficiency	22%			

Table 5: Effect of the higher-mass analysis cuts on the data and a signal for $h_{30\ GeV/c^2} \to \tau\tau$, $A_{40\ GeV/c^2} \to b\bar{b}$ in the $\tau^+\tau^- jj$ MSSM analysis.

Cut	Individually			Cumulatively		
	Data	Signal	s/n	Data	Signal	s/n
Generated	–	2000	–	–	2000	–
Preselection	1886	858	1.0	1886	858	1.0
C1H) $E_{pair} > 4.55\ GeV$	1189	790	1.7	1189	790	1.7
C2H) $E_{cone} < 2\ GeV$	605	546	2.0	491	527	2.5
C3H) $\cos\theta_{pair-p(total)} < 0.8$	1481	811	1.2	325	504	3.7
C4H) $Sphericity > 0.1$	597	819	3.0	51	497	25.5
C5H) $cos(\theta_{open}) < 0.6$	291	737	5.6	0	477	–

Table 6: Effect of the lower-mass analysis cuts on the data and a signal for $h_{12\ GeV/c^2} \to \tau\tau$, $A_{25\ GeV/c^2} \to b\bar{b}$ in the $\tau^+\tau^- jj$ MSSM analysis.

Cut	Individually			Cumulatively		
	Data	Signal	s/n	Data	Signal	s/n
Generated	–	2000	–	–	2000	–
Preselection	1886	1072	1.0	1886	1072	1.0
C1L) $E_{pair} > 9.1\ GeV$	697	809	2.0	697	809	2.0
C2L) $E_{cone} < 2\ GeV$	438	834	3.3	270	668	4.4
C3L) $N_{track}^{hemi} = 2$	215	714	5.8	94	542	10.1
C4L) $cos(\theta_{open}) < 0.95$	830	1021	2.1	19	534	49.4
C5L) $\cos\theta_{pair-p(total)} < 0.8$	1481	984	1.2	10	489	86.0
C6L) $Sphericity > 0.04$	1089	972	1.6	0	439	–

Table 7: Effect of the selection cuts (applied sequentially to the data) on the data, QCD background, and for a signal $h_{35\ GeV/c^2}$, $A_{40\ GeV/c^2} \to b\bar{b}b\bar{b}$ in the 4-jet MSSM analysis. The Monte Carlos are described in the text.

Cut	Data	QCD MC	Signal
Generated	26099	47000	1000
D1) $Thrust < 0.85$	2952	5406	952
D2) $N_{jet} = 4$	553	877	354
D3) $\bar{M} < 7.5\ GeV/c^2$, $\bar{D} < 5.0\ GeV/c^2$	229	350	237
D4) Kinematics	110	178	193
D5) Acoplanarity	10	24	94

Table 8: Preselection efficiencies for the data and for various Monte Carlo samples (sequential cuts applied to the full samples) in the 4 jet MSSM analysis.

Sample	Thrust cut	4-jet requirement
Data	0.113 ± 0.002	0.032 ± 0.001
JETSET(detailed)	0.118 ± 0.003	0.028 ± 0.002
HERWIG(detailed)	0.115 ± 0.005	0.034 ± 0.003
JETSET(sp.1)	0.115 ± 0.004	0.029 ± 0.002
JETSET(sp.2)	0.115 ± 0.004	0.032 ± 0.002
JETSET(sp.3)	0.112 ± 0.004	0.029 ± 0.002
JETSET(sp.4)	0.116 ± 0.004	0.031 ± 0.002
ALL Monte Carlo	0.115	0.030
$\pm$ r.m.s. scatter	± 0.002	± 0.002

Table 9: Selection efficiencies for the data and for various Monte Carlo samples (which were normalized to the data after the preselection cuts) in the 4 jet MSSM analysis. The numbers shown are the reduction factors obtained by applying the cuts D3,D4, and D5 sequentially, as in Table 7.

Sample	Jets	(D3)	(D4)	(D5)
Data	0.66 ± 0.03	0.42 ± 0.02	0.43 ± 0.02	0.16 ± 0.02
JETSET(detailed)	0.65 ± 0.05	0.44 ± 0.04	0.41 ± 0.04	0.13 ± 0.02
HERWIG(detailed)	0.66 ± 0.06	0.38 ± 0.05	0.41 ± 0.05	0.19 ± 0.03
JETSET(sp.1)	0.58 ± 0.05	0.46 ± 0.05	0.40 ± 0.04	0.19 ± 0.03
JETSET(sp.2)	0.65 ± 0.05	0.42 ± 0.04	0.46 ± 0.04	0.20 ± 0.03
JETSET(sp.3)	0.58 ± 0.05	0.43 ± 0.04	0.47 ± 0.04	0.21 ± 0.03
JETSET(sp.4)	0.59 ± 0.05	0.38 ± 0.04	0.46 ± 0.04	0.21 ± 0.03
ALL Monte Carlo	0.617	0.422	0.438	0.195
$\pm$ r.m.s. scatter	± 0.035	± 0.028	± 0.029	± 0.030

Figures

Figure 1. Distribution of p_T for the data (points) and JETSET events (histogram) after cuts A1-4; the Monte Carlo has been normalized to the luminosity. The excess of data at low p_T is due to two-photon processes which are not modelled in the Monte Carlo.

Figure 2. $E_{forward}/E_{all}$ versus $E_{backward}$, for the MSM search, after cuts A1-5. The data are shown in a), while MC events for a 24 GeV/c^2 H^0 are shown in b). The final cuts are indicated in the upper left corners.

Figure 3. Expected number of events, as a function of MSM Higgs boson mass. The dashed line shows the number of events expected from the channel $H^0 \to q\bar{q}$, $Z^{0*} \to \nu\bar{\nu}$, while the dotted line is the number expected from $H^0 \to q\bar{q}$, $Z^{0*} \to (e^+e^-$ *or* $\mu^+\mu^-)$; the solid line is the sum of these modes, reduced by the systematic uncertainty. The horizontal line indicates the levels expected for the 95% confidence level upper limit.

Figure 4. Excluded Higgs masses (95% C.L. limits) for the MSSM searches in the parameter space m_h *vs* m_A. Since $m_h \leq m_A$, region A is excluded. Curve B (dashed line) represents the limits obtained from the Minimal Standard Model Higgs boson search. Curves C (solid line; "H" and "L" for high- and low-mass analyses, respectively) are obtained using the $\tau^+\tau^-$ *jet jet* mode; the region between the curves and the diagonal $m_h = m_A$ is excluded. Curve D (dotted line) represents the limit obtained from the 4 jet search. Curve E shows the region excluded using the 4 τ mode. The dip at $m_h = 9.5 - 10.5$ GeV/c^2 indicates the resonance region where the branching fraction $h^0 \to \tau^+\tau^-$ could be suppressed at the χ_b masses, and region F (shaded) could contain points which are not excluded if the τ production is highly supressed for both the h^0 and A^0. Curves B and D are valid for all values of $\tan\beta$, while C and E are valid only for $\tan\beta > 1$. The regions of the plot which are *not* excluded by the present anaylsis are indicated by shading.

Figure 5. Energy of the $\tau^+\tau^-$ decay products, after the pre-selection cuts of the $h^0A^0 \to \tau^+\tau^-b\bar{b}$ (higher mass) analysis. a) Data (points) and JETSET MC (histogram). b) Signal for $m_h = 30$, $m_A = 40$ GeV/c^2. The shaded histogram shows events in which the analysis identified the correct pair of tracks from the $\tau^+\tau^-$ system.

Figure 6. Sum of unassociated electromagnetic energy in a cone of $\cos\theta = 0.3$ about the pair axis, after the pre-selection cuts of the $h^0A^0 \to \tau^+\tau^-b\bar{b}$ (higher mass) analysis. a) Data (points) and JETSET MC (histogram). b) Signal for $m_h : m_A = 30 : 40$ GeV/c^2. The shaded histogram shows events in which the analysis identified the correct pair of tracks from the $\tau^+\tau^-$.

Figure 7. Cosine of the angle between the $\tau^+\tau^-$ pair and the missing energy direction, after the pre-selection cuts of the $h^0A^0 \to \tau^+\tau^-b\bar{b}$ (higher mass) analysis. a) Data (points) and JETSET MC (histogram). b) Signal for $m_h : m_A = 30 : 40$ GeV/c^2. The shaded histogram shows events in which the analysis identified the correct pair of tracks from the $\tau^+\tau^-$.

Figure 8. Sphericity distribution of the event, after the pre-selection cuts of the $h^0A^0 \to \tau^+\tau^-b\bar{b}$ (higher mass) analysis. a) Data (points) and JETSET MC (histogram). b) Signal for $m_h : m_A = 30 : 40$ GeV/c^2. The shaded histogram shows events in which the analysis identified the correct pair of tracks from the $\tau^+\tau^-$.

Figure 9. Cosine of the $\tau^+\tau^-$ pair opening angle. after the pre-selection cuts of the $h^0A^0 \to \tau^+\tau^-b\bar{b}$ analysis. a) Data (points) and JETSET MC (histogram). b) Signal for $m_h : m_A = 30 : 40$ GeV/c^2. The shaded histogram shows events in which the analysis identified the correct pair of

tracks from the $\tau^+\tau^-$.

Figure 10. Distribution of $\bar{M}$, after cuts D1,2 of the $h^0A^0 \to b\bar{b}b\bar{b}$ analysis. a) Data (points) and JETSET MC (histogram); the Monte Carlo has been normalized to the data after the preselection cuts. b) Signal for $m_h : m_A = 35 : 40\ GeV/c^2$.

Figure 11. Distribution of $\bar{D}$, after cuts D1,2 of the $h^0A^0 \to b\bar{b}b\bar{b}$ analysis. a) Data (points) and JETSET MC (histogram). b) Signal for $m_h : m_A = 35 : 40\ GeV/c^2$.

Figure 12. Distribution of acoplanarity for charged tracks, after cuts D1-4 of the $h^0A^0 \to b\bar{b}b\bar{b}$ analysis. a) Data (points) and JETSET MC (histogram). b) Signal for $m_h : m_A = 35 : 40\ GeV/c^2$.

Figure 13. Distribution of acoplanarity for electromagnetic clusters, after cuts D1-4 of the $h^0A^0 \to b\bar{b}b\bar{b}$ analysis. a) Data (points) and JETSET MC (histogram). b) Signal for $m_h : m_A = 35 : 40\ GeV/c^2$.

Figure 14. Excluded Higgs masses for the MSSM searches in the parameter space m_h *vs* $\tan(\beta)$. The regions enclosed by the curves are excluded at the 95% C.L.. Curve B represents the limits obtained from the Minimal Standard Model Higgs boson search. Curve C is obtained using the $\tau^+\tau^-$ *jet jet* mode ("high mass analysis"). Curve D is the limit obtained from the 4 jet search.

Figure 1

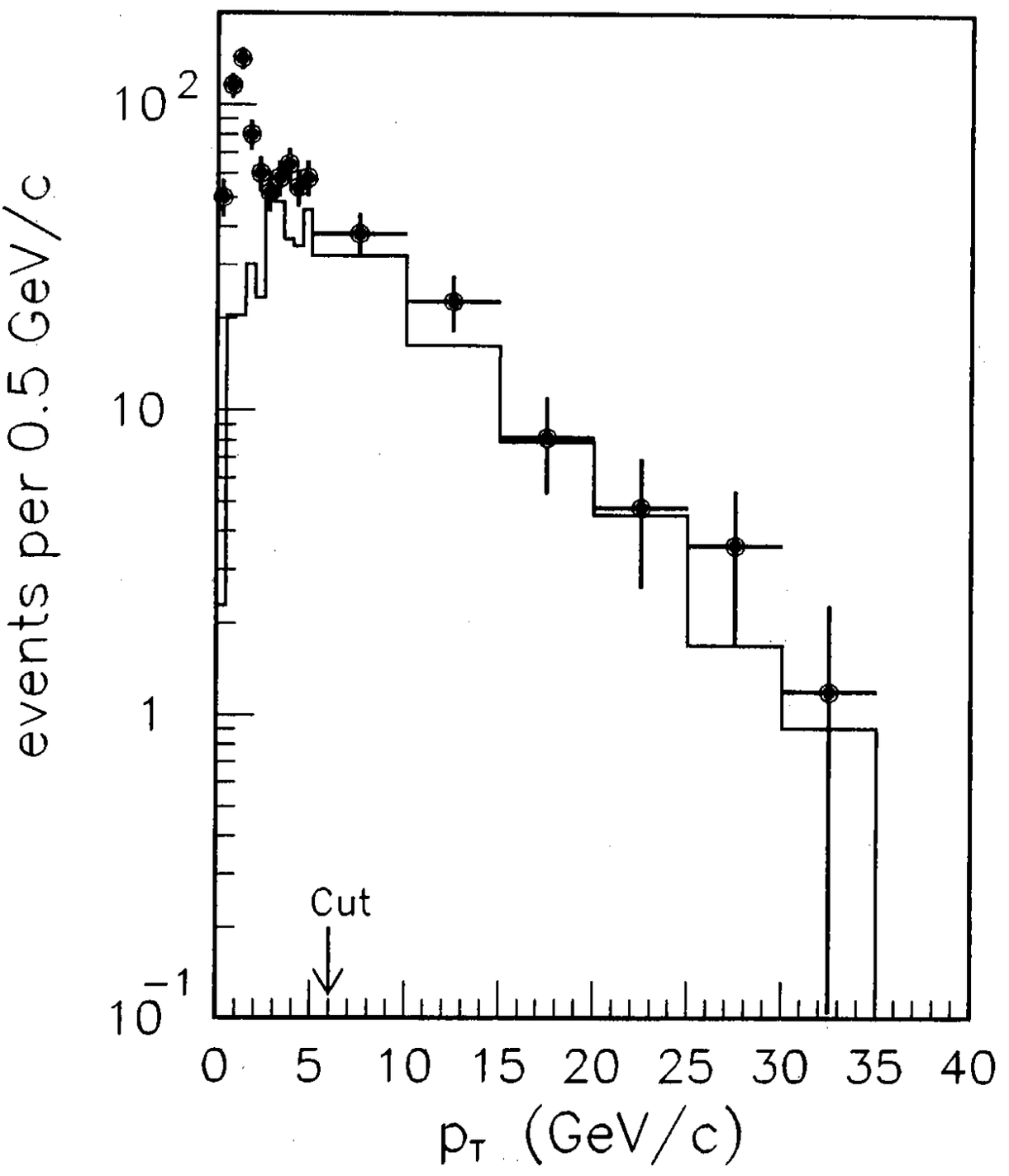

Figure 2

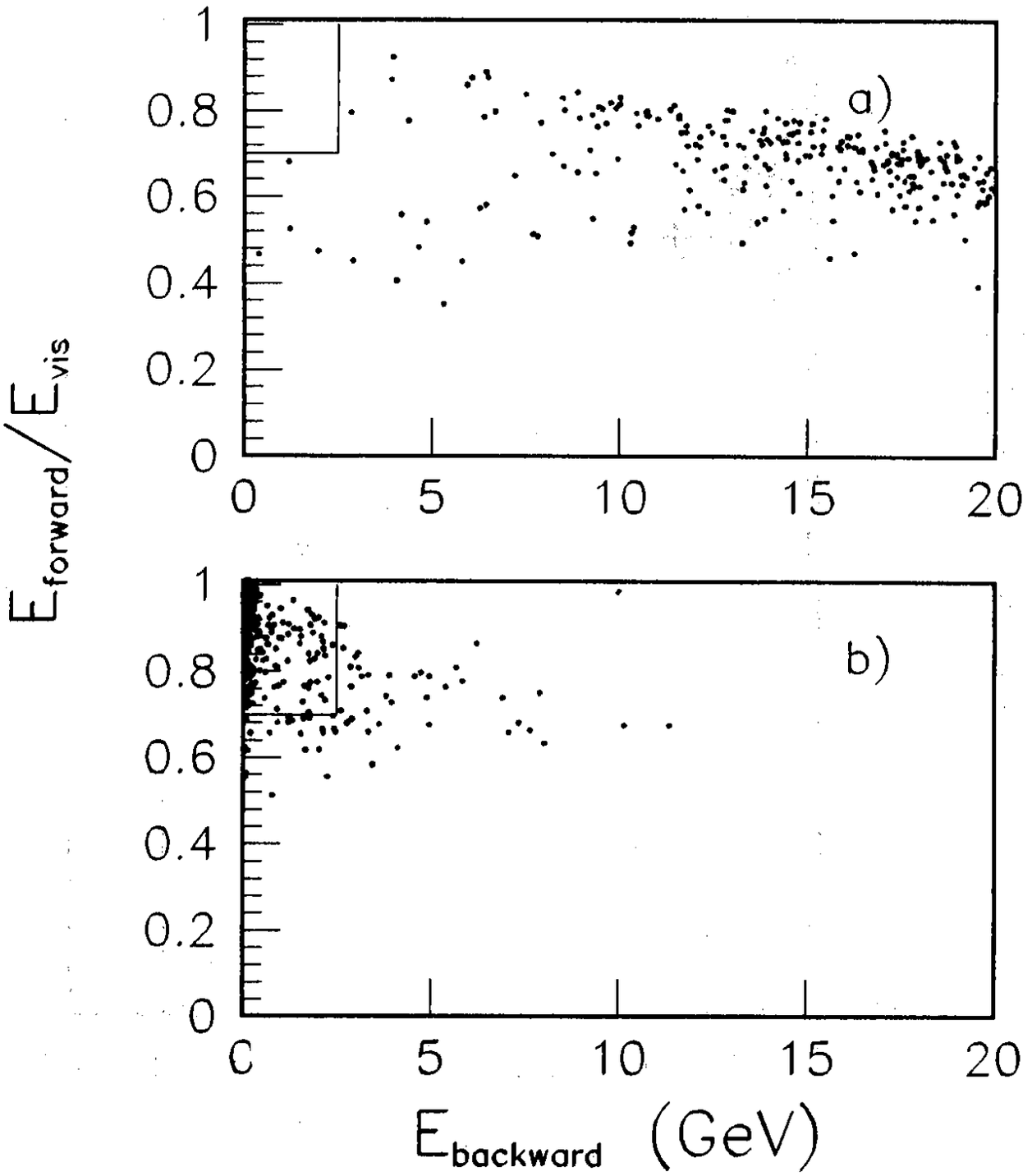

Figure 3

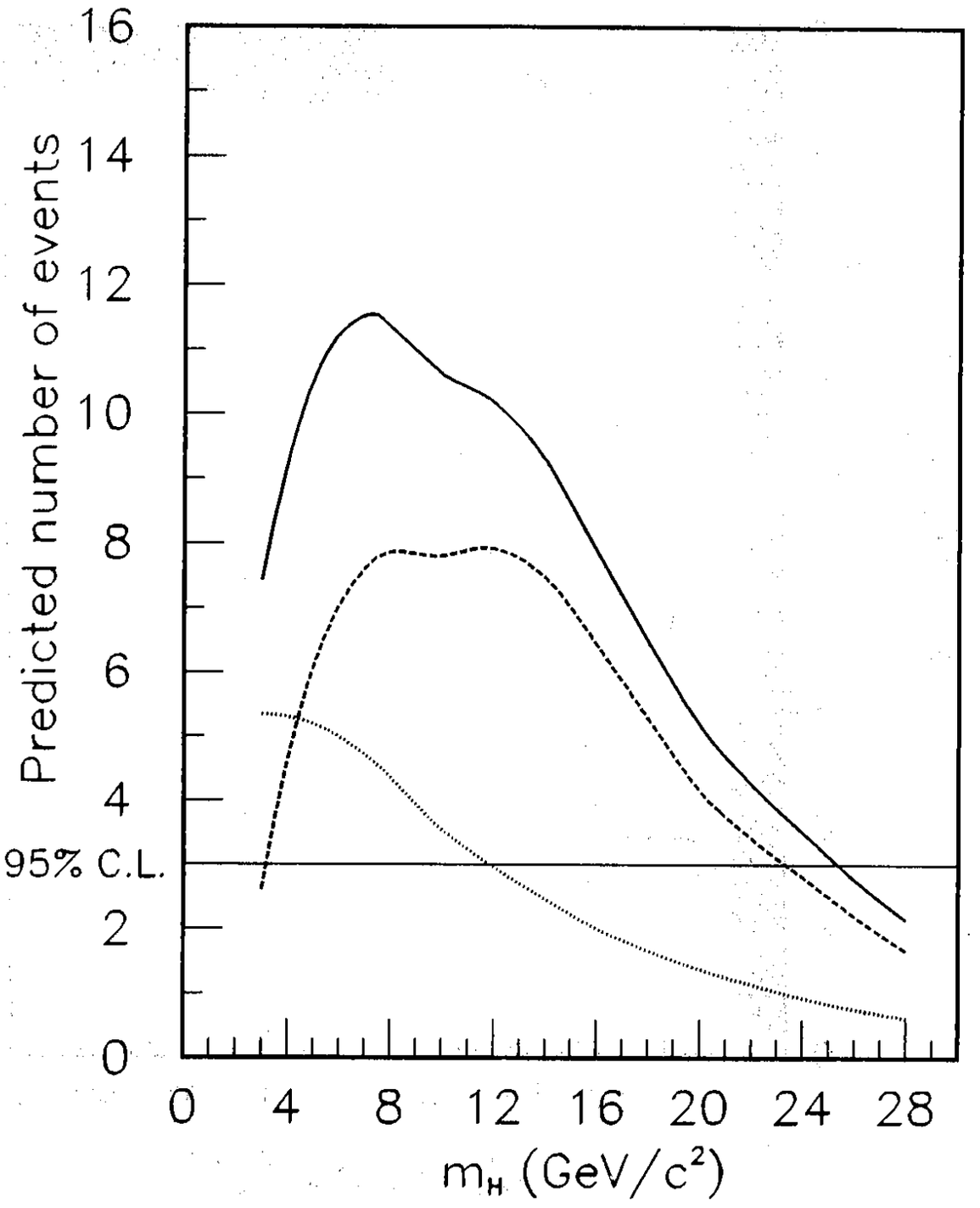
Predicted number of events
16
14
12
10
8
6
4
95% C.L.
2
0
0
4
8
12
16
20
24
28
m_H (GeV/c^2)

Figure 4

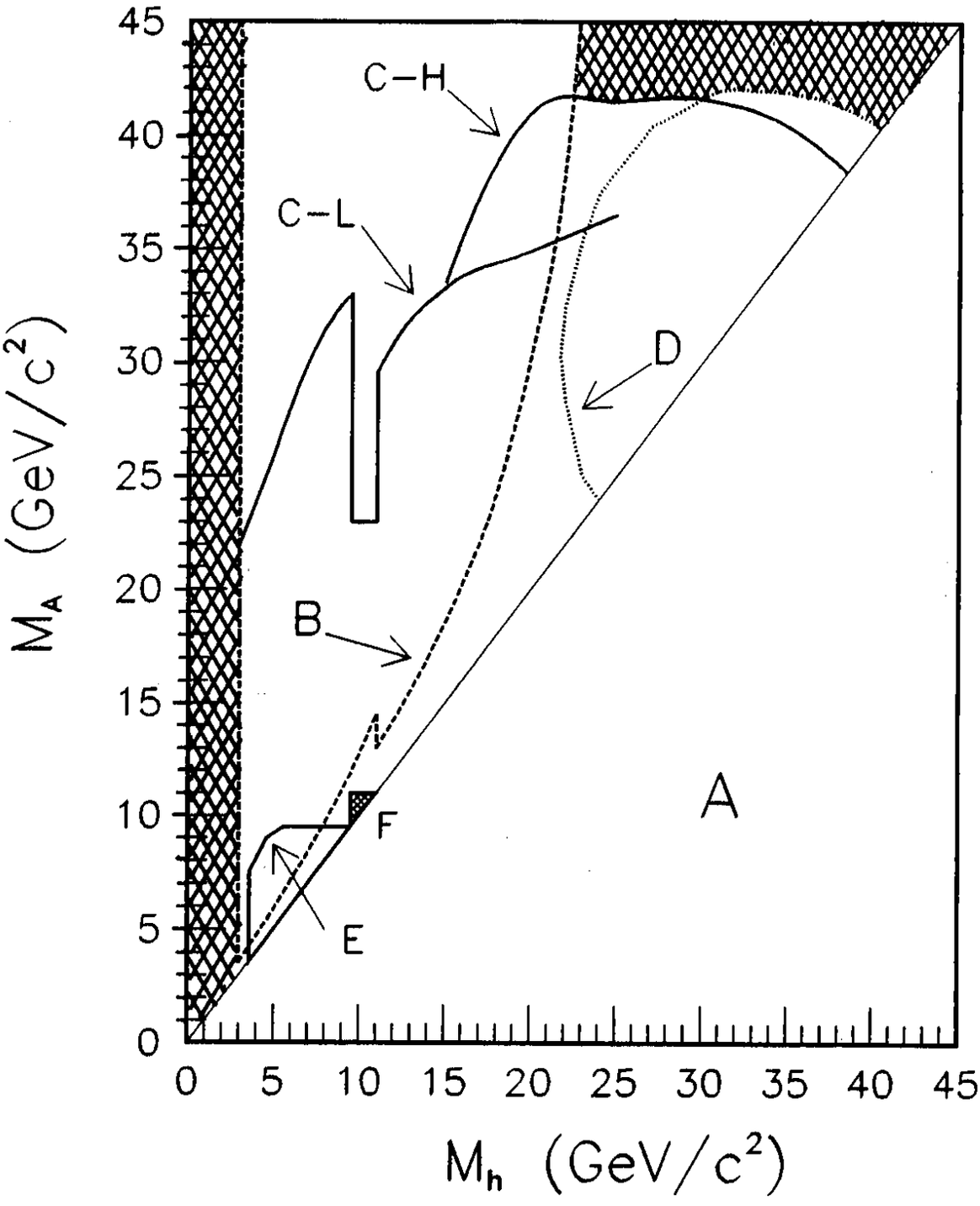
45
40
35
30
25
20
15
10
5
0
0
5
10
15
20
25
30
35
40
45
C–H
C–L
D
B
A
F
E
M_A (GeV/c^2)
M_h (GeV/c^2)

Figure 5

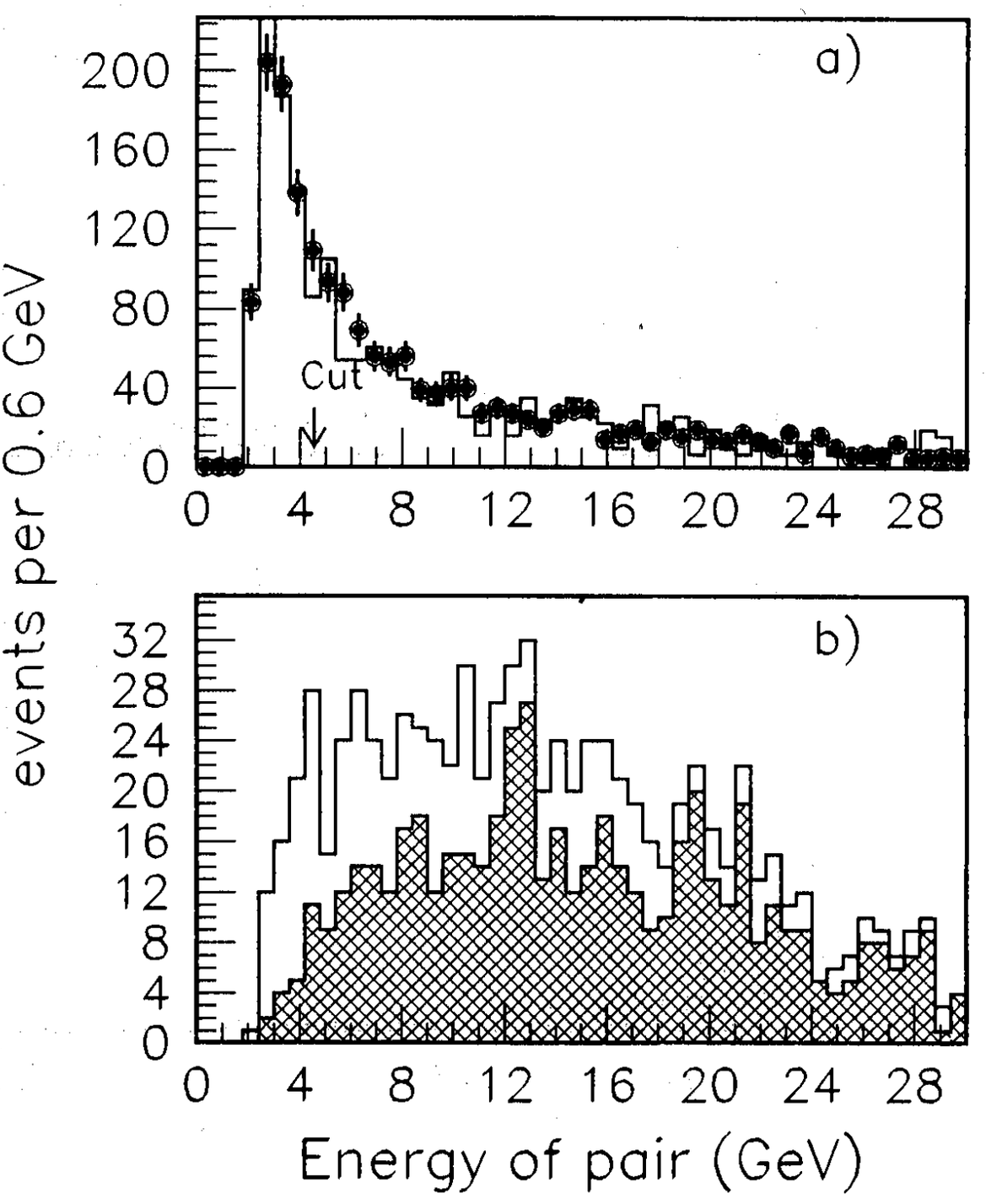
a)
b)
Cut
events per 0.6 GeV
Energy of pair (GeV)
0
40
80
120
160
200
4
8
12
16
20
24
28
32

Figure 6

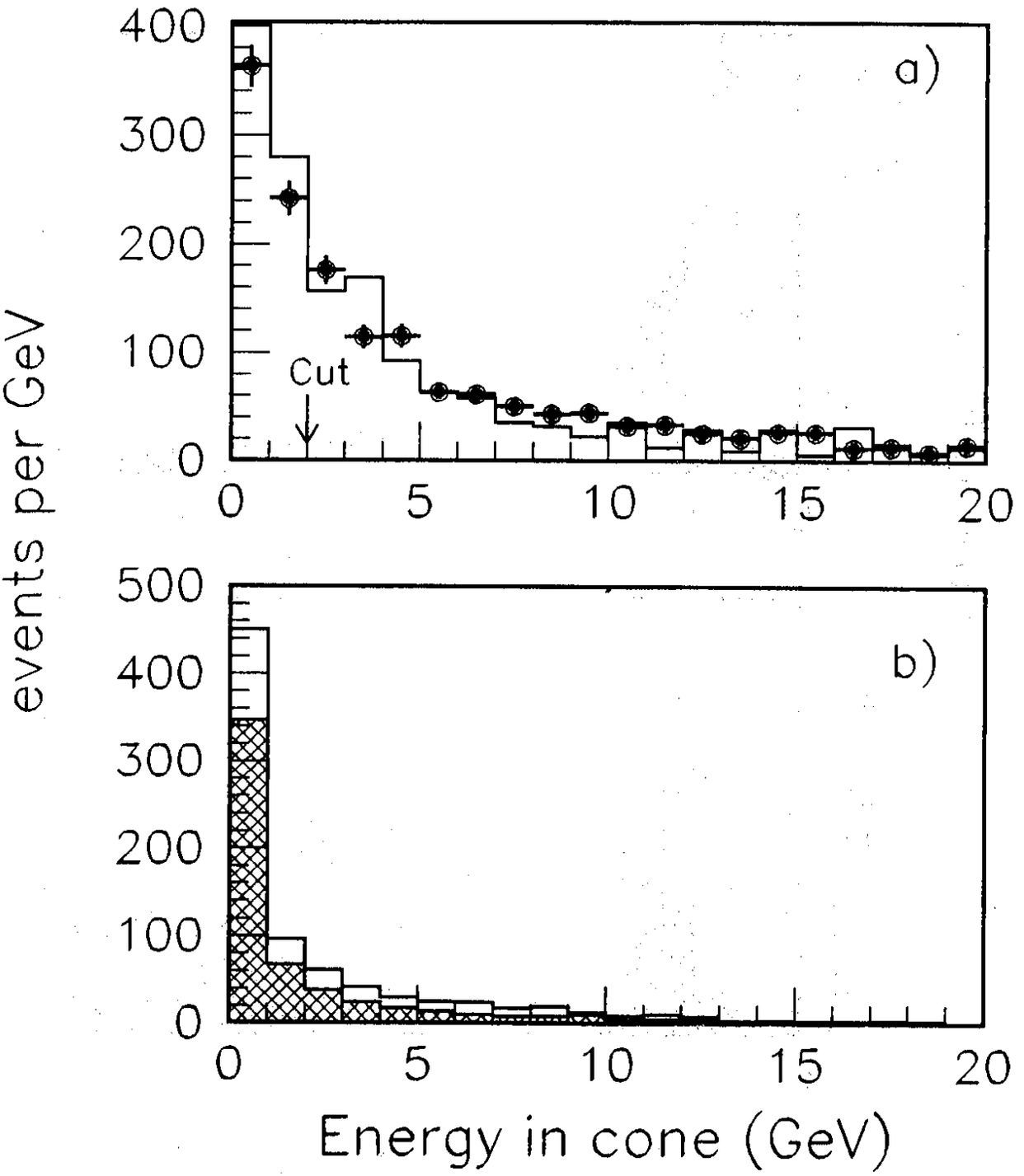
400
300
200
100
0
a)
Cut
0
5
10
15
20
500
400
300
200
100
0
b)
0
5
10
15
20
events per GeV
Energy in cone (GeV)

Figure 7

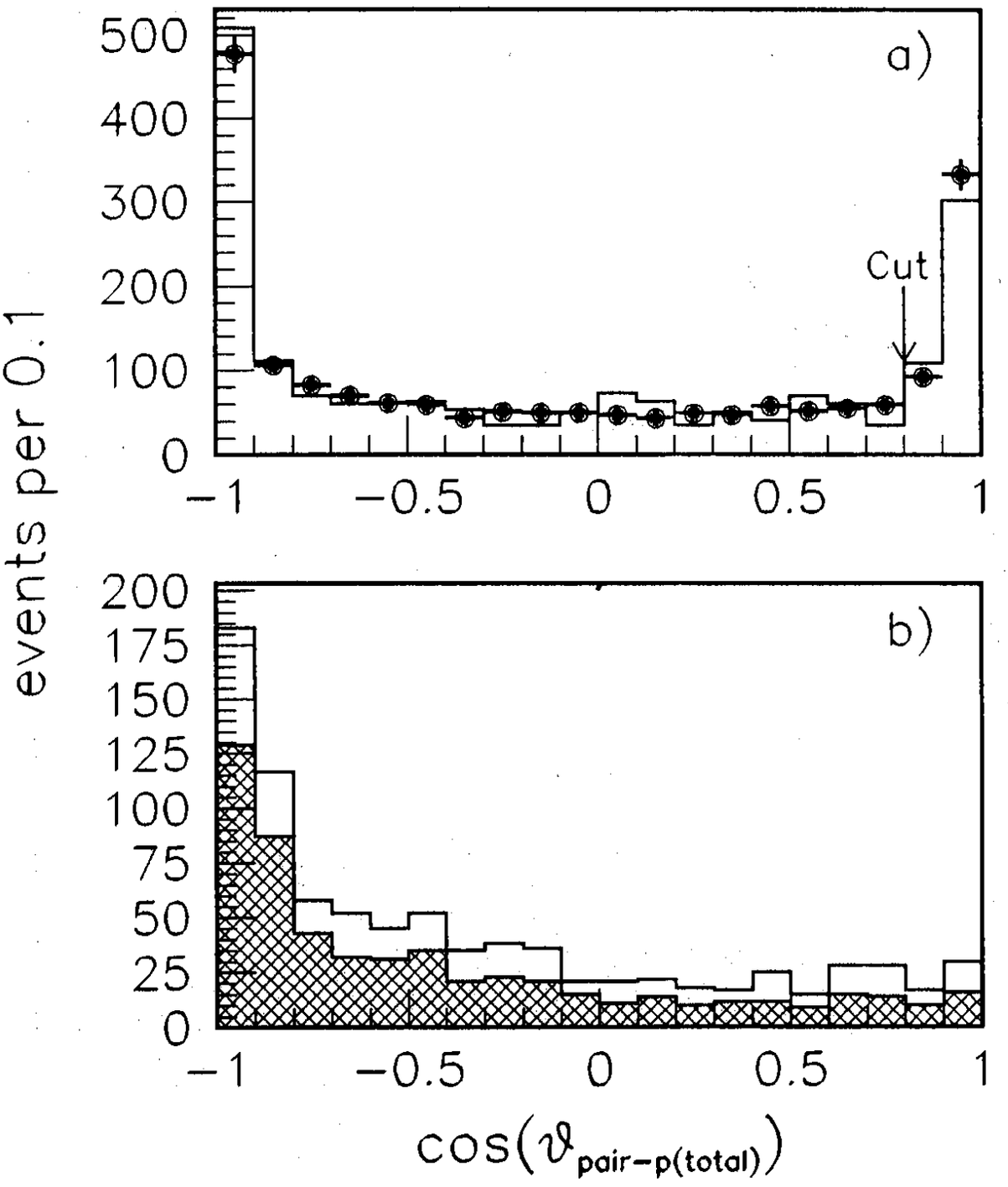
a)
Cut
b)
events per 0.1
500
400
300
200
100
0
200
175
150
125
100
75
50
25
0
−1
−0.5
0
0.5
1
cos(ϑ pair−p(total))

Figure 8

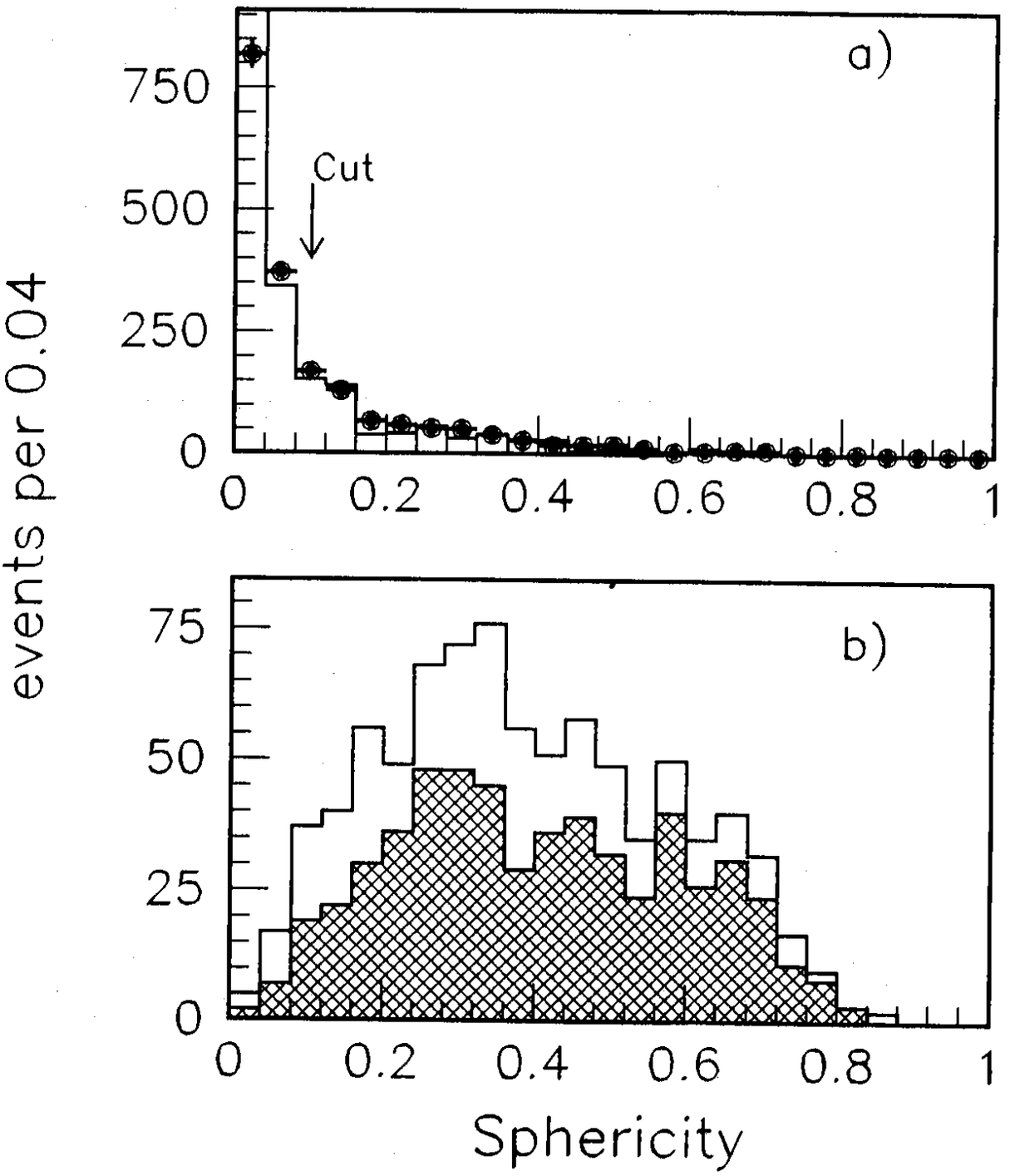
a)
Cut
750
500
250
0
0
0.2
0.4
0.6
0.8
1
b)
75
50
25
0
0
0.2
0.4
0.6
0.8
1
events per 0.04
Sphericity

Figure 9

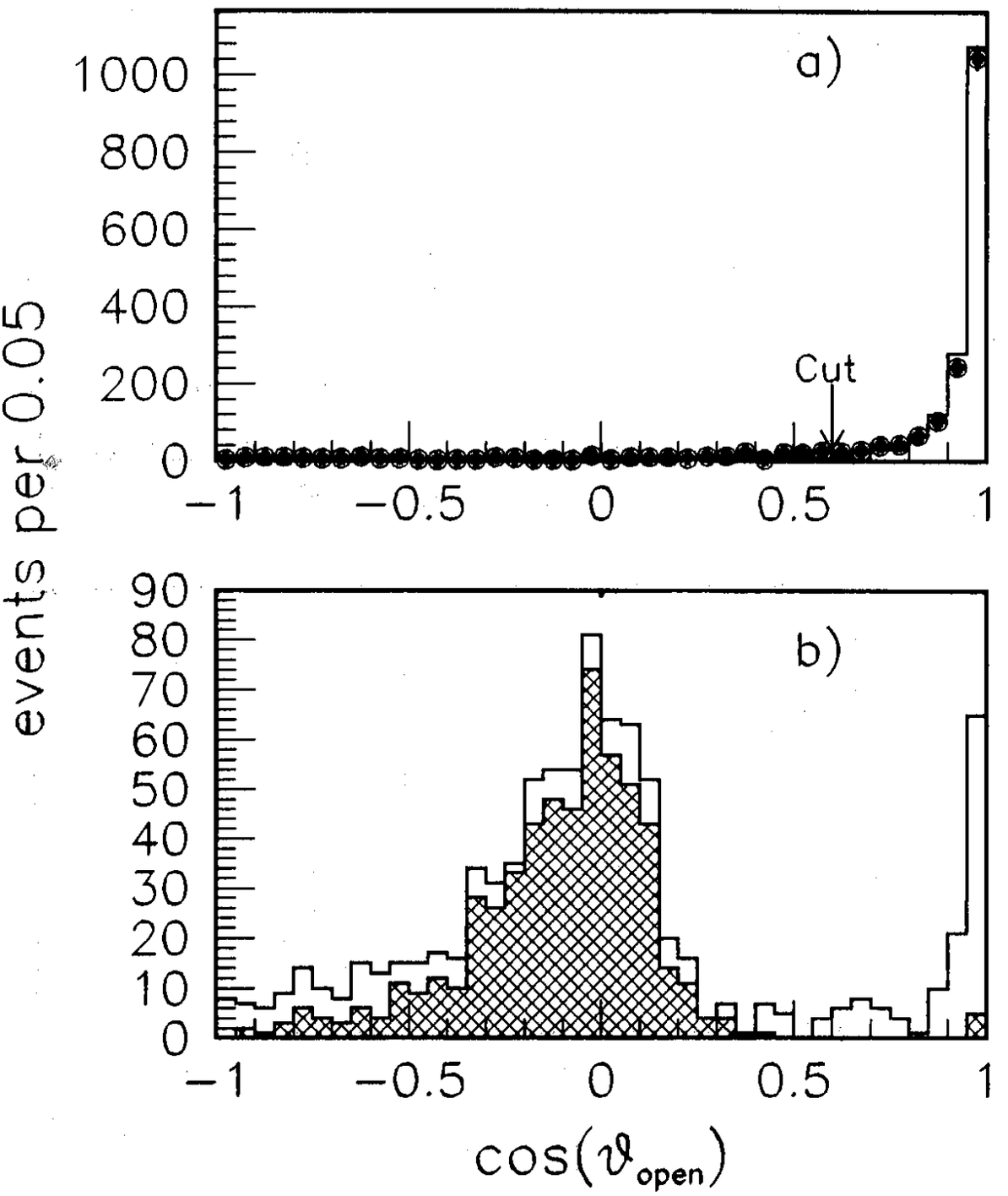
a)
b)
Cut
events per 0.05
1000
800
600
400
200
0
90
80
70
60
50
40
30
20
10
0
−1
−0.5
0
0.5
1
cos(ϑ open)

Figure 10

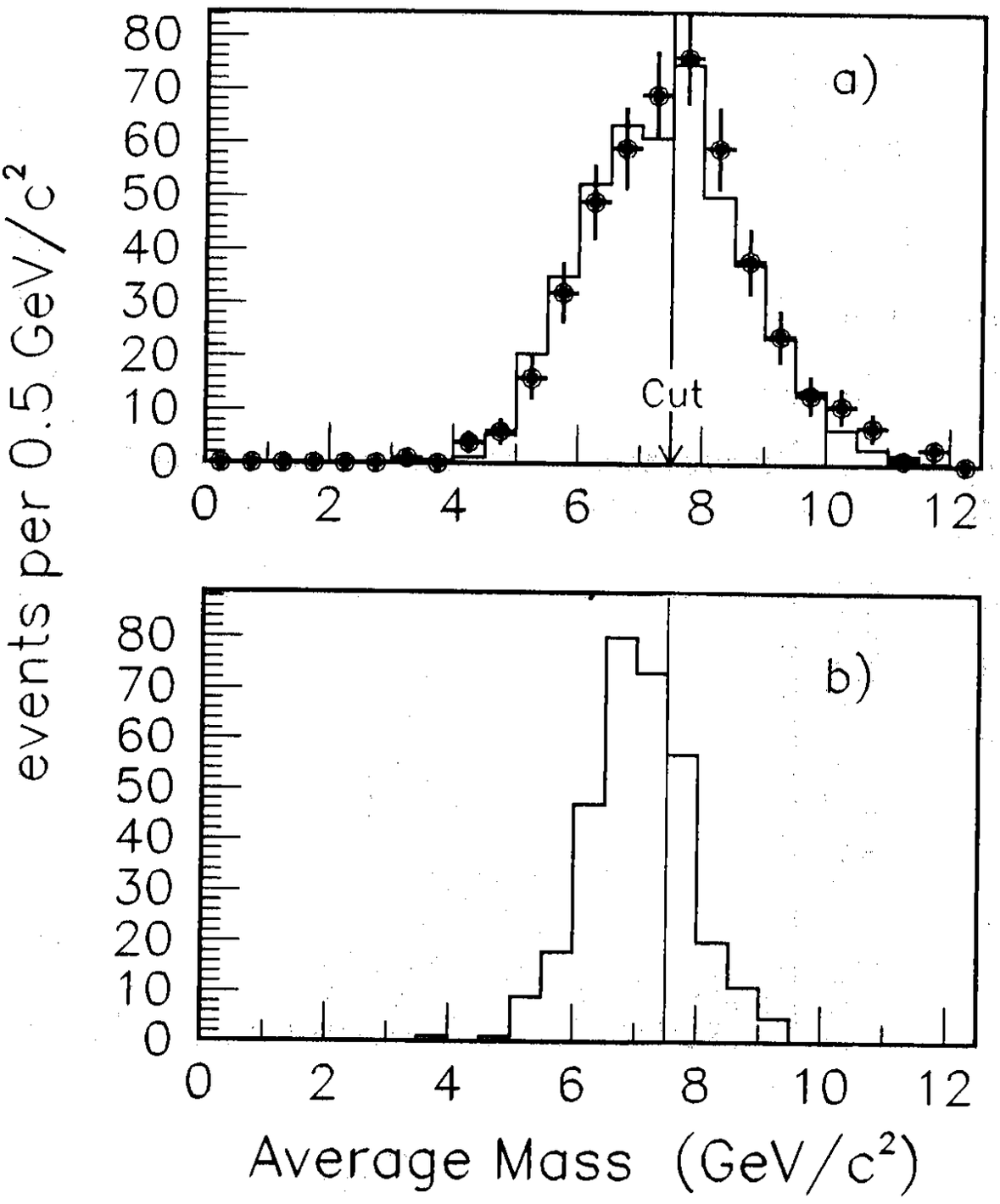
a)
b)
Cut
events per 0.5 GeV/c²
Average Mass (GeV/c²)
0
10
20
30
40
50
60
70
80
0
2
4
6
8
10
12

Figure 11

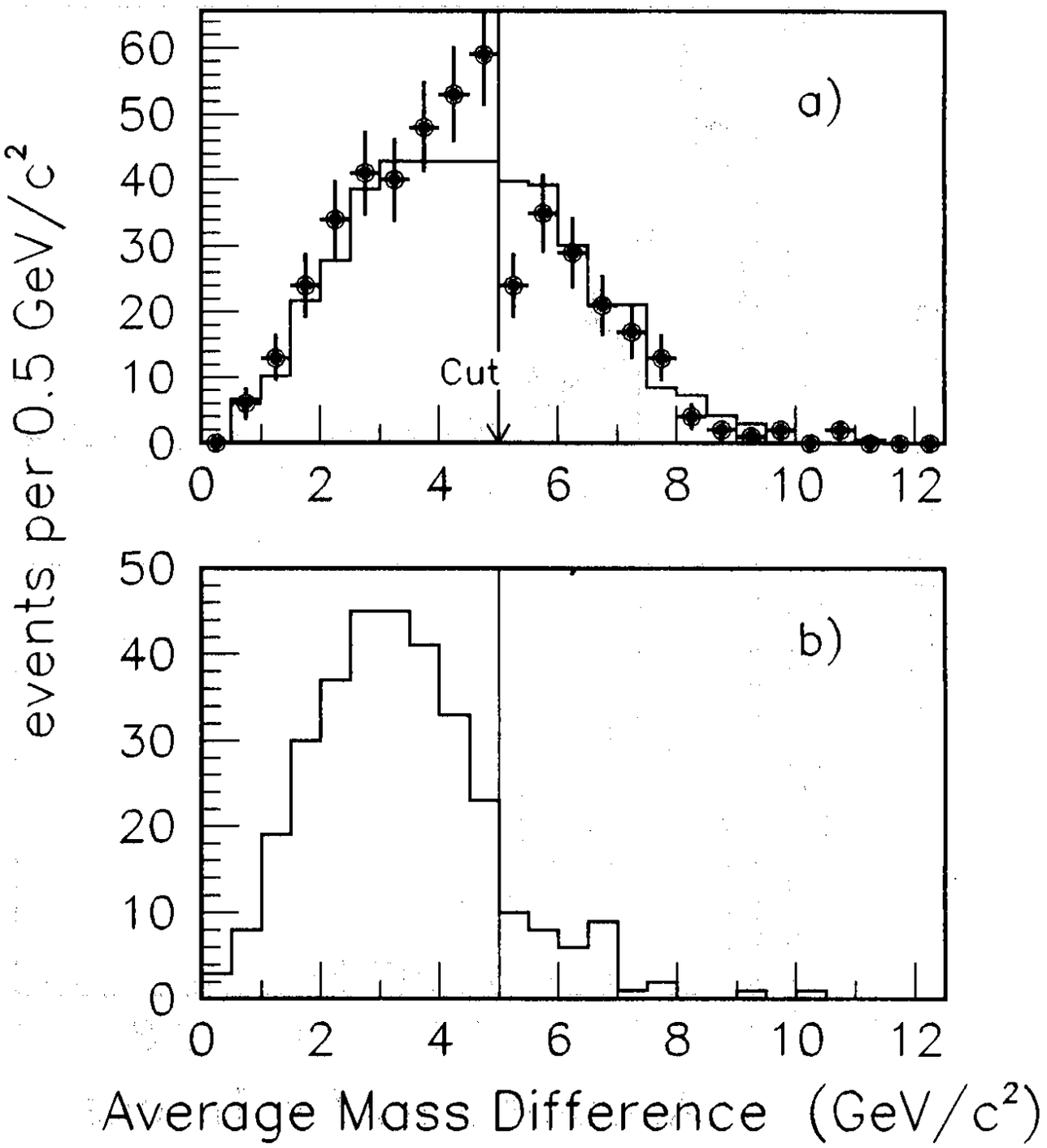
a)
b)
Cut
events per 0.5 GeV/c²
Average Mass Difference (GeV/c²)
0
10
20
30
40
50
60
0
2
4
6
8
10
12

Figure 12

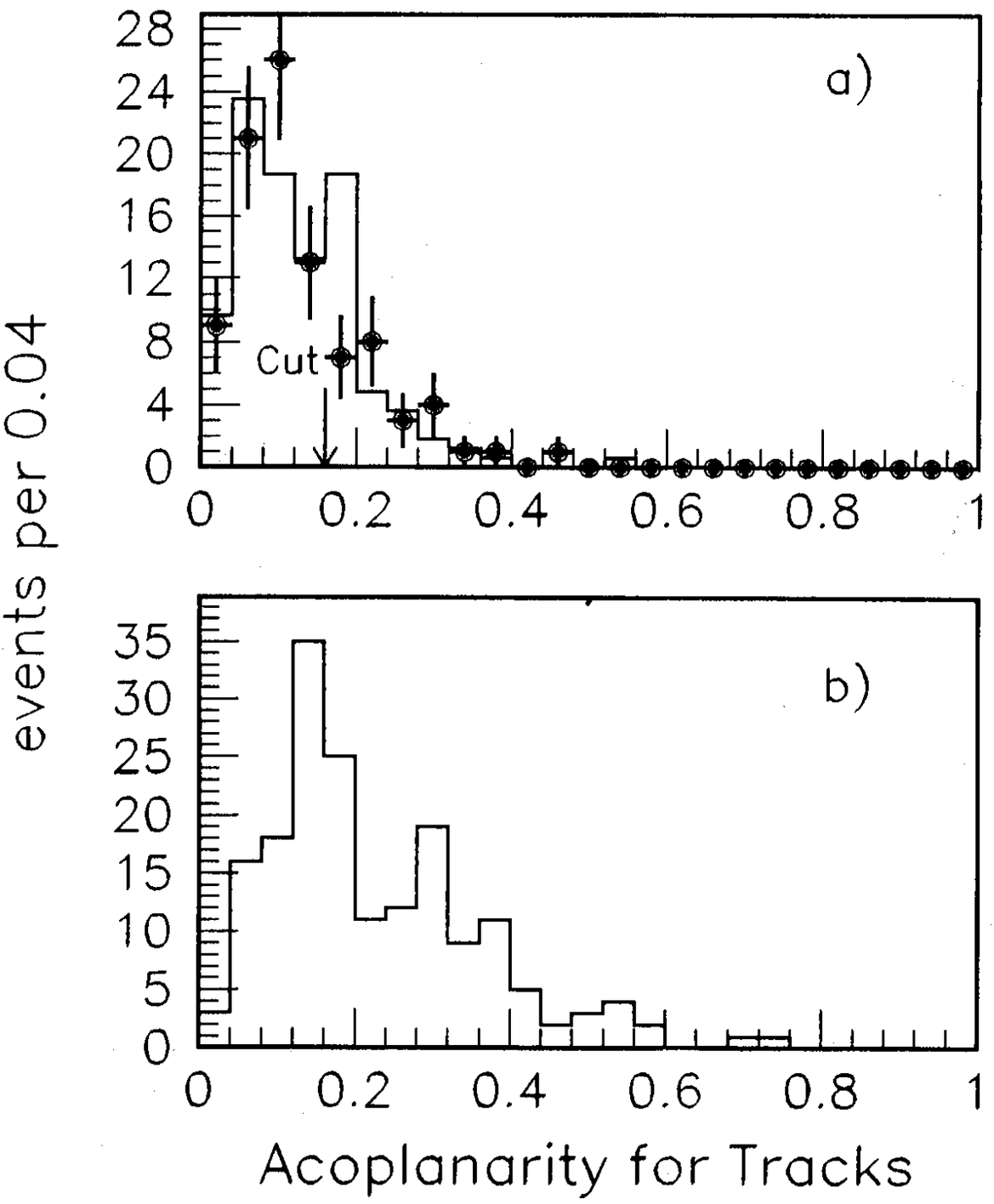
a)
b)
Cut
events per 0.04
Acoplanarity for Tracks
0
4
8
12
16
20
24
28
5
10
15
25
30
35
0.2
0.4
0.6
0.8
1

Figure 13

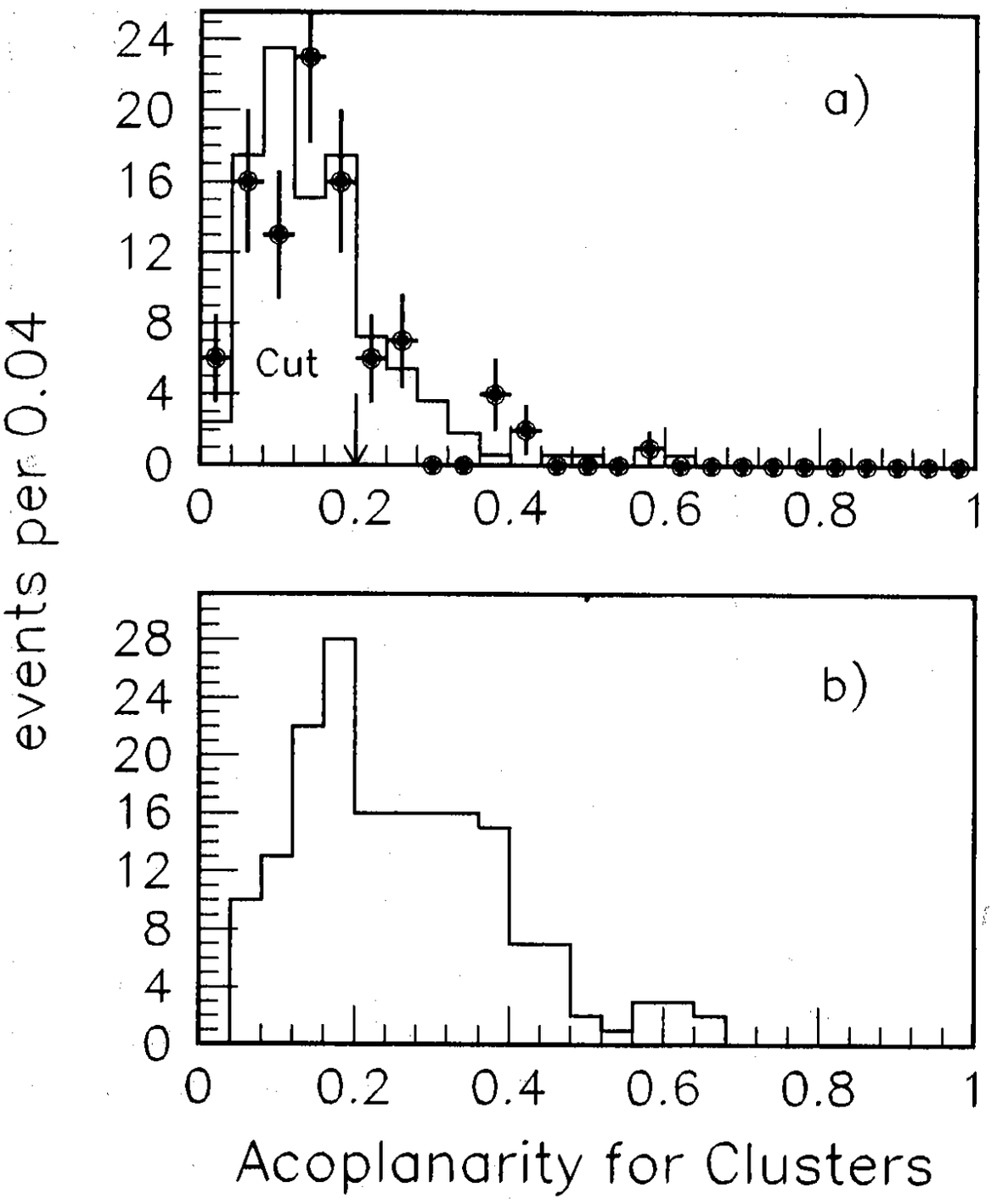
a)
Cut
b)
events per 0.04
Acoplanarity for Clusters
0
4
8
12
16
20
24
28
0.2
0.4
0.6
0.8
1

Figure 14

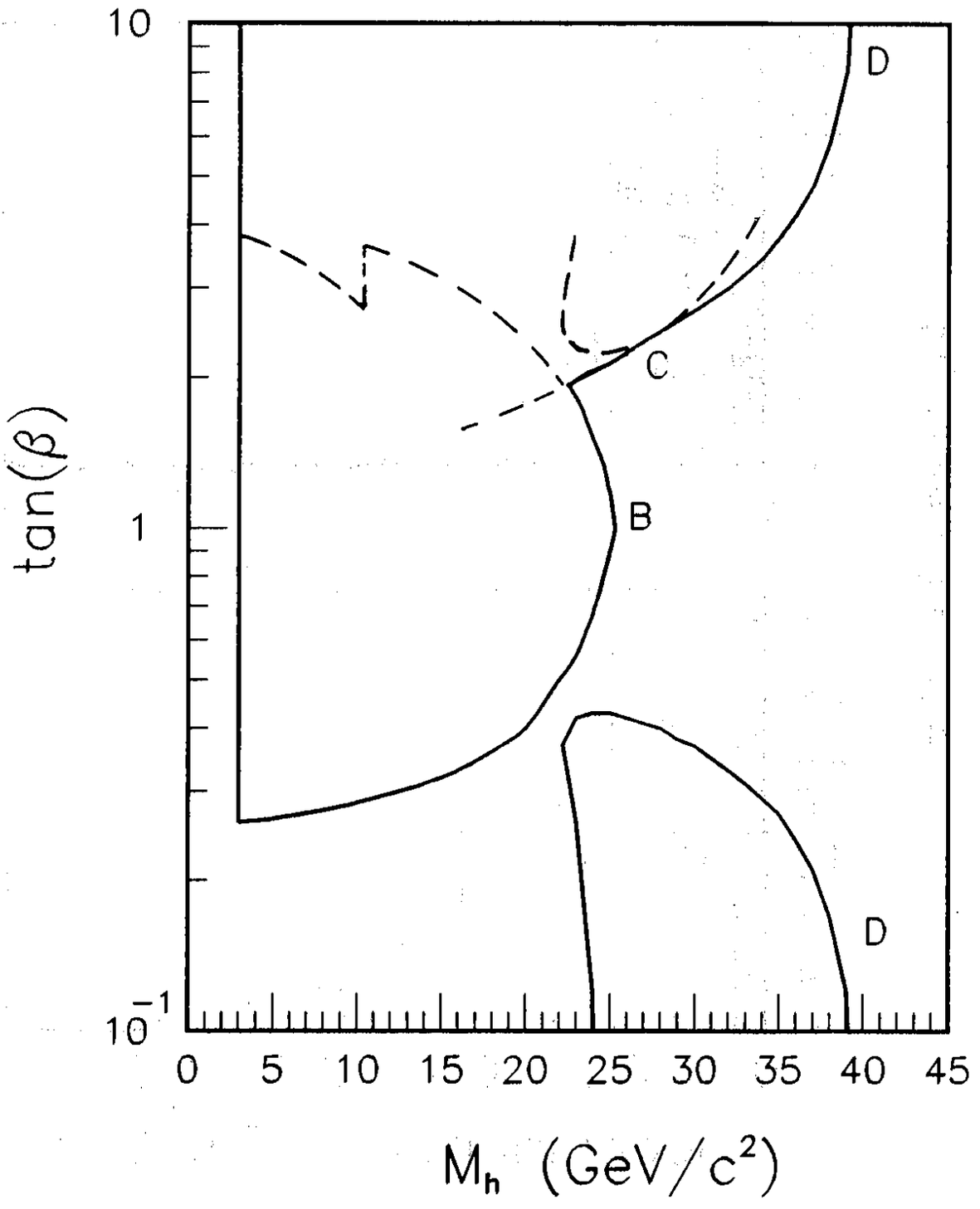

Imprimé au CERN. Prix : 0.80 Fr.